© 2022. Published by The Company of Biologists Ltd | Journal of Experimental Biology (2022) 225, jeb244151. doi:10.1242/jeb.244151

RESEARCH ARTICLE

Vectored jets power arms-first and tail-first turns differently in brief squid with assistance from fins and keeled arms

Ian K. Bartol[1,*], Alissa M. Ganley[1], Amanda N. Tumminelli[1], Paul S. Krueger[2] and Joseph T. Thompson[3]

ABSTRACT

Squids maneuver to capture prey, elude predators, navigate complex habitats and deny rivals access to mates. Despite the ecological importance of this essential locomotive function, limited quantitative data on turning performance and wake dynamics of squids are available. To better understand the contribution of the jet, fins and arms to turns, the role of orientation (i.e. arms first versus tail first) in maneuvering, and the relationship between jet flow and turning performance, kinematic and 3D velocimetry data were collected in tandem from brief squid, *Lolliguncula brevis*. The pulsed jet, which can be vectored to direct flows, was the primary driver of most turning behaviors, producing flows with the highest impulse magnitude and angular impulse about the main axis of the turn (yaw) and secondary axes (roll and pitch). The fins and keeled arms played subordinate but important roles in turning performance, contributing to angular impulse, stabilizing the maneuver along multiple axes and/or reducing rotational resistance. Orientation affected turning performance and dynamics, with tail-first turns being associated with greater impulse and angular impulse, longer jet structures, higher jet velocities and greater angular turning velocities than arms-first turns. Conversely, arms-first turns involved shorter, slower jets with less impulse, but these directed short pulses resulted in lower minimum length-specific turning radii. Although the length-to-diameter ratio (*L*/*D*) of ejected jet flow was a useful metric for characterizing vortical flow features, it, by itself, was not a reliable predictor of angular velocity or turning radii, which reflects the complexity of the squid multi-propulsor system.

KEY WORDS: *Lolliguncula brevis*, Turning, Maneuverability, Velocimetry, Kinematics, Hydrodynamics

INTRODUCTION

Although rectilinear swimming has been the primary focus of most prior aquatic locomotion studies, unsteady swimming maneuvers that involve directional and rotational changes are common and can dominate activity budgets (Webb, 1991, 1997, 2006; Boisclair and Tang, 1993; Tang et al., 2000). Maneuvering in the aquatic realm is critical for capturing prey and eluding predators, navigating spatially complex habitats, and even denying rivals access to mates (Moody et al., 1983; Ehlinger and Wilson, 1988; Howland, 1974; Weihs and Webb, 1984; Domenici and Blake, 1997; Hanlon and Messenger, 2018). Given the importance of turning for a swimmer's locomotive toolkit, maneuvering has received recent attention in a wide range of taxa, including fishes (Fish et al., 2018; Thankdiackal and Lauder, 2020; Parson et al., 2011), marine mammals (Leahy et al., 2021), birds (Clifton and Biewener, 2018), siphonophores (Sutherland et al., 2019), jellyfishes (Gemmell et al., 2015; Dabiri et al., 2020) and squids (Jastrebsky et al., 2016; 2017).

While many of the turning performance studies have centered on kinematic approaches, fewer studies have focused on quantifying flow around active swimmers. Measuring flow around multiple propulsors and control surfaces during maneuvers is not trivial, but it is an important step for calculating structure-specific force and moment magnitudes and directions. By linking body movements with their momentum consequences, it is possible to understand which types of motion are most effective for maneuvering. Indeed, flow quantification work has identified some key principles for turning, such as the importance of strong forces at bell margins in jellyfishes for generating torque (Gemmell et al., 2015), the significance of tuning the velar aperture and angle for maneuvering and reversing in siphonophores (Sutherland et al., 2019), the influence of laterally directed flows from pectoral fins in trout and sunfish (Drucker and Lauder, 2001, 2003), and the relevance of mechanical work done by the fluid on anterior/middle regions of the body of zebrafish (Thankdiackal and Lauder, 2020).

Squids swim and maneuver using a combination of pulsed jetting, fin motions and arm positioning. The pulsed jet is capable of vectoring flows in different directions using mantle contractions and a flexible funnel (Bartol et al., 2001b, 2009a,b), while the fins can both oscillate and undulate to varying degrees depending on the locomotive mode (Anderson and DeMont, 2005; Bartol et al., 2001b, 2018). During swimming and turning maneuvers, the arms can bend, lengthen and contract, and a muscular keel that runs the length of some arms can be extended or retracted (Bartol et al., 2001b; Hanlon and Messenger, 2018; Jastrebsky et al., 2016; see Kier, 1982, for schematic diagram of an arm keel). Using these muscular hydrostatic systems (Kier, 1989; Kier and Smith, 1985; Kier and Thompson, 2003), squids can turn in a forward (arms-first, AF) or backward (tail-first, TF) direction with small turning radii, rapidly reverse course mid-turn, and even vertically twirl (Hanlon et al., 1983; Vecchione and Roper, 1991; Bartol et al., 2001a,b; Jastrebsky et al., 2016). These behaviors involve multiple propulsors (fins and jet) and control surfaces (arms and fins) that generate complex 3D flows. To decouple contributions from these systems, 3D flow and kinematic quantification are required.

For this study, we explored 3D wake dynamics and associated kinematics of the brief squid, *Lolliguncula brevis*, during turning, with the goal of addressing several driving questions. (1) What are the relative contributions of the jet, fins and arms to turning performance? Given that inshore squids rely more heavily on the jet than on the fins for steady swimming (O'Dor, 1988; Bartol et al., 2001b; Anderson and Grosenbaugh, 2005) and a rotatable jet

[1]Department of Biological Sciences, Old Dominion University, Norfolk, VA 23529, USA. [2]Department of Mechanical Engineering, Southern Methodist University, Dallas, TX 75275, USA. [3]Department of Biology, Franklin and Marshall College, Lancaster, PA 17604, USA.

*Author for correspondence (ibartol@odu.edu)

I.K.B., 0000-0001-9006-8727

Received 18 February 2022; Accepted 29 June 2022

Journal of Experimental Biology (2022) 225, jeb244151. doi:10.1242/jeb.244151

List of symbols and abbreviations

A	angular impulse
$\mathbf{A}_{pitch}$	angular impulse about the pitch axis
$\mathbf{A}_{roll}$	angular impulse about the roll axis
$\mathbf{A}_{yaw}$	angular impulse about the yaw axis
AF	arms-first swimming (i.e. swimming in the forward direction)
COR	center of rotation
DML	dorsal mantle length
I	linear impulse
I	total impulse magnitude
L/D	length to diameter ratio of jet
L_v/D_ω	velocity-based jet length divided by vorticity-based jet diameter
L_ω/D_ω	vorticity-based jet length divided by vorticity-based jet diameter
R	radius of the turning path
R/L	COR radius divided by total length of the animal
R/L_{mean}	average of the COR radii for a turn divided by total length of the animal
R/L_{min}	90th percentile minimum R/L
TF	tail-first swimming (i.e. swimming in the rearward direction)
u	velocity vector
U_{jave}	average jet velocity
U_{jmax}	peak jet velocity
x	position vector
θ_{DV}	dorsoventral arm angle
θ_L	lateral arm angle
θ_M	mantle angle
θ_{yaw}	angle of body relative to the x-axis in the x–z plane
ρ	fluid density
$\boldsymbol{\omega}$	vorticity vector
Ω	angular velocity
Ω_{max}	90th percentile maximum Ω
Ω_{mean}	mean angular velocity throughout turn

facilitates course changes, we hypothesized that most of the angular impulse for turning is provided by the jet compared with the other systems. This hypothesis was tested by quantifying flows from the jet, fins and arms using 3D velocimetry. (2) Does swimming orientation (AF versus TF) affect turning hydrodynamics and performance? We hypothesized that squid turning AF produce short jet pulses that facilitate tighter (smaller radius) turns, while squid turning TF produce long, powerful jets that contribute to faster (higher angular velocity) turns. These predictions are based on isolated jet vortex rings being more prevalent in AF than in TF rectilinear swimming (Bartol et al., 2016) and sharp turns being recorded as squid approach prey in the AF mode (Jastrebsky et al., 2017). To test this hypothesis, we compared jet properties (e.g. length, velocity, impulse) and kinematic parameters (e.g. turning radius, angular velocity) for AF and TF turns. (3) Are hydrodynamic jet flow properties predictive of turning performance? The length to diameter ratio (L/D) of a jet is an important metric, as it is linked to the physical limit of vortex ring formation, propulsive performance and thrust augmentation (Gharib et al., 1998; Krueger and Gharib, 2003; Bartol et al., 2009a). We predicted that lower L/D (shorter jets) will correlate closely with small turning radii and higher L/D (longer jets) will correlate with high angular velocities, irrespective of turning orientation. To address this question, we compared L/D and other jet properties with turning performance variables across all turns.

MATERIALS AND METHODS

Animals

Brief squid, *Lolliguncula brevis* (Blainville 1823) [N=68; dorsal mantle length (DML)=5.1–9.2 cm; total length (TL) (mantle length+head+arms, determined from video)=7.9–14.2 cm] were captured in Wachapreague, VA, USA, by otter trawl and transported to Old Dominion University's Marine Aquatics Facility in Norfolk, VA, USA, in aerated coolers. Animals were maintained in 1700 l recirculating seawater systems at 30 ppt and 24°C. They were fed grass shrimp *Palaemonetes pugio* following protocols described in Hanlon et al. (1983) and Bartol et al. (2009a). Animals were allowed to acclimate for at least 48 h prior to experimentation.

Experiments

All experiments were performed in a 38 l glass tank filled with filtered seawater matching the conditions of the holding tanks and laden with reflective seeding particles (polyamide, 50 µm, Dantec Dynamics, Skövlunde, Denmark) (Fig. 1A). The reflective particles were illuminated with a pulsed Brilliant B Twins 380 mJ, 532 nm, 10 Hz laser (Quantel Laser, Bozeman, MT, USA) for 3D flow quantification (see below). To illuminate the squid body, several halogen lights with filters for transmitting light at red (>600 nm) wavelengths were used, with each light mounted to an aluminium frame positioned around the viewing tank. Three Falcon cameras (Teledyne Dalsa, Inc., Waterloo, ON, Canada; 1400×1200 pixels, 100 frames s^{-1}), each outfitted with notch filters to block 532 nm laser illumination, were positioned around the working section to record behaviors in lateral and dorsal views. Likewise, the V3V-8000 probe (TSI, Inc., Shoreview, MN, USA; three 2048×2048 pixel cameras, 15 frames s^{-1}, 14×14×10 cm sampling volume) used for flow field quantification was configured with optical filters to block out the red lighting and allow only laser light illumination (532±5 nm) to reach the sensors.

Each squid was added to the viewing tank and allowed to acclimate for 5–15 min under aerated conditions. Following acclimation, aeration was discontinued, and experiments commenced with the simultaneous recording of 3D velocimetry data and kinematic data for 1 min recording runs. The number of recording runs varied from 5 to 25, depending on the cooperativity of the test animal. For some squid that spent time at the tank edges, a net was used to gently guide the animals in the direction of the laser volume; however, all turns within the sample volume were spontaneous and unaided by the net. We used defocusing digital particle tracking velocimetry (DDPTV) to quantify three-component velocity field measurements in a volumetric domain (Bartol et al., 2016, 2018; Couch and Krueger, 2011; Gharib et al., 2002; Kajitani and Dabiri, 2005; Pereira and Gharib, 2002, 2004; Pereira et al., 2006). Using INSIGHT 4G V3V software, a synchronizer and the V3V-8000 probe (TSI, Inc.), paired images of flows around the squid were captured at 5 Hz (the Q-switch frequency of the dual laser system described above). The time separation between paired images (Δt) ranged from 0.5 to 2.0 ms. Video acquisition and recording from the Falcon cameras was achieved using a DVR Express CORE2 system (IO Industries, London, ON, Canada). For each recording run, 300 paired velocimetry images and 6000 kinematic images (per camera) were collected.

Kinematic processing

One turning sequence each from 68 squid was selected for kinematic processing (29 AF sequences and 39 TF sequences). The chosen sequences met the following criteria: turns were away from tank walls, squid were not visibly startled by the laser, and the sequences included high-quality DDPTV data, with well-developed vortical flow features. For each of these turning sequences, position tracking of squid body landmarks was performed using image-tracking software (DLTdv7; Hedrick, 2008). Both lateral and dorsal views were considered in this analysis, and the tracking protocols were similar to those described

Journal of Experimental Biology (2022) 225, jeb244151. doi:10.1242/jeb.244151

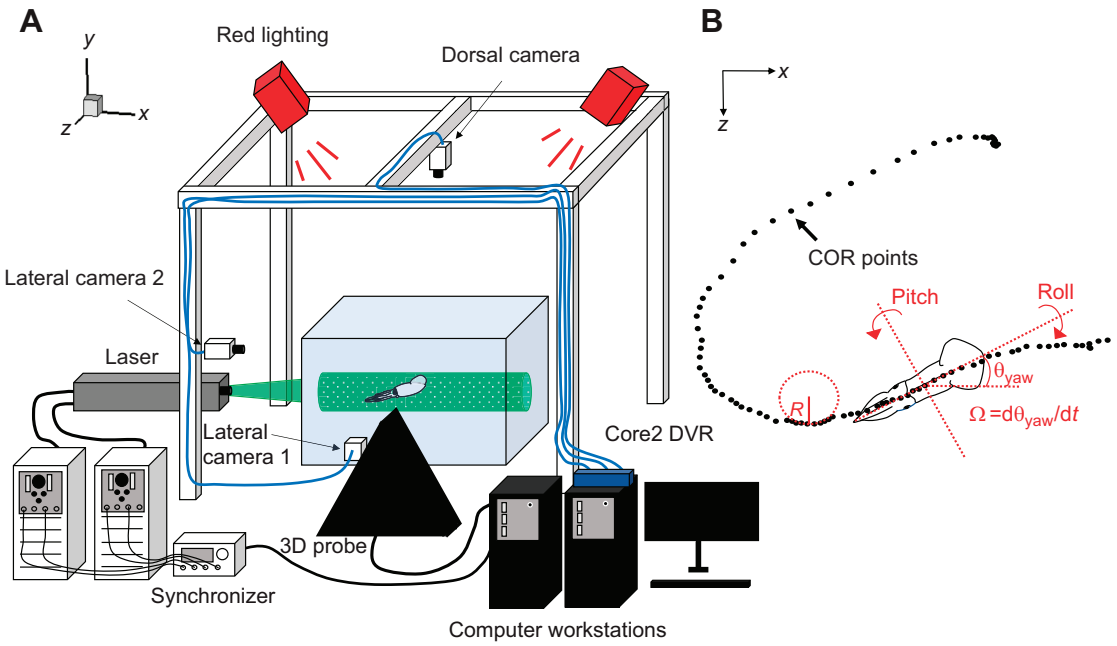

Fig. 1. Experimental design. Illustration of experimental setup (A) and center of rotation (COR) points for a squid turning counterclockwise with yaw angle and pitch/roll axes shown (B). The radius (*R*) of the COR path is measured throughout the turn and divided by the total length of the animal (*L*) to calculate length-specific radii of the turns (*R*/*L*). The numerical derivative of the animal θ_{yaw} versus time was determined using a fourth-order finite difference formula to compute angular velocity (Ω).

in Jastrebsky et al. (2016). For dorsal footage, the tail tip, midpoint between the eyes, arm tip, right/left mantle margin and right/left fin tips were digitized, whereas for lateral footage, the tail tip, eye, arm tip and fin tip were tracked (Fig. 2C,F). Digitized points in the video footage were used to determine the center of rotation (COR), angular velocity (Ω), mantle angle (θ_M), dorsoventral arm angle (θ_{DV}), lateral arm angle (θ_L), mantle contraction frequency and fin beat frequency using in-house MATLAB routines or Microsoft Excel (Figs 1B and 2). θ_M was the acute angle of the mantle with the horizontal in the lateral view, θ_{DV} was the angle between the mantle and arms in the lateral view, and θ_L was the angle between the mantle and arms in the dorsal view (Fig. 2). COR data were

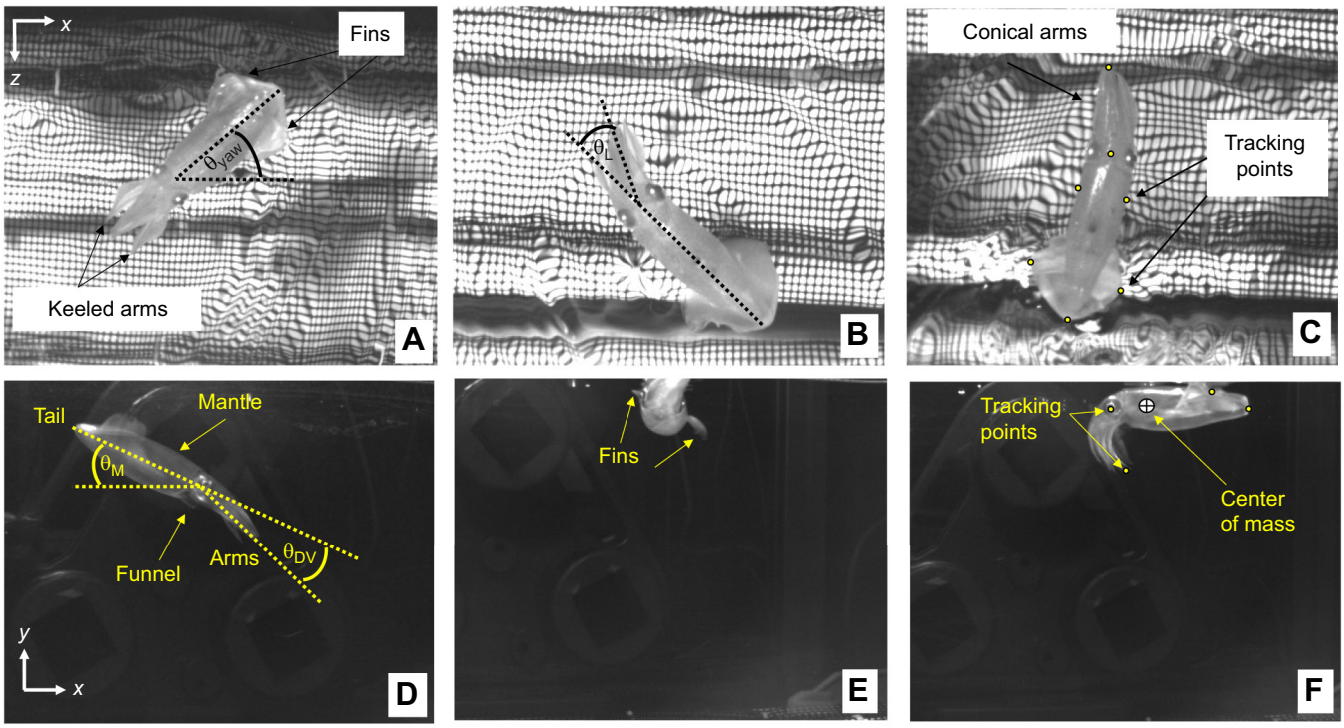

Fig. 2. Video frames of brief squid, *Lolliguncula brevis*, during turning sequences. (A–C) Dorsal camera perspective; (D–F) lateral camera perspective. Yaw angle (θ_{yaw}), lateral arm angle (θ_L), mantle angle (θ_M) and dorsoventral arm angle (θ_{DV}) are depicted in A, B and D. Dorsal points used for kinematic tracking are shown in C, lateral points are shown in F along with the squid's center of mass.

Journal of Experimental Biology (2022) 225, jeb244151. doi:10.1242/jeb.244151

smoothed using the mean squared error (MSE) algorithm (Walker, 1998).

The COR is the point in the domain of the squid body that moves the least during the turn. The COR was located on a line that is at a fixed angle from the line connecting the tail tip and arm tip and that has the same length as the distance between these points. The COR position on this line and the angle of the line are selected so that the COR moves the least amount during the turn. The radius (R) of the turning path is the radius of curvature of the COR path/trajectory (Fig. 1B). This was computed from analytical geometry using:

$$\frac{1}{R} = \frac{z''}{(1+(z')^2)^{3/2}}, \quad (1)$$

where $z'=\mathrm{d}z/\mathrm{d}x=\dot{z}/\dot{x}$, $z''=\mathrm{d}^2z/\mathrm{d}x^2=(\dot{x}\ddot{z}-\ddot{x}\dot{z})/\dot{x}^3$, x and z are the coordinates of the COR in the dorsal view, t is time, the dot-over represents time differentiation, and the derivatives were evaluated using fourth-order accurate finite difference equations. To compare our data with those of previous studies, radius of the turning path (R) was divided by the total length of the animal to determine a length-specific turning radius (R/L). R/L_{mean} is the average of all COR radii for a given turn, divided by the total length of the animal, whereas Ω_{mean} is the mean angular velocity throughout the turn. To account for frame digitization error, turning radii and angular velocities for each sequence were ranked, and the 90th percentile minimum R/L (R/L_{min}) and the 90th percentile maximum Ω (Ω_{max}) were determined.

DDPTV processing

Within a turning sequence, the DDPTV image(s) that captured the most developed flow field effecting the turn, i.e. where vorticity had completely shed from the propulsor or control surface and where impulse and angular impulse were maximal for the turn, was processed. For some sequences where multiple propulsors/control surfaces were involved, the most developed flow field occurred over two frames, and thus separate frames were used for impulse calculations of the different propulsors (Fig. 3). Using 1–2 frames with the most developed flow fields for the turn is reasonable because these images contain the cumulative history of the flow generation, and calculation of impulse and angular impulse are integral methods. Given that illuminated regions of the squid body can lead to erroneous velocity vectors, a MATLAB routine or custom mask was used to remove the brightly lit squid body from the DDPTV particle field images prior to processing. Velocity and vorticity fields were calculated using INSIGHT 4G V3V software, and 3D isosurface plots were generated using Tecplot 360 (Tecplot, Bellevue, WA, USA). Details on the processing parameters used may be found in Bartol et al. (2016, 2018). Generally, 18,000–25,000 particle vectors were obtained within the sampling volume, and a voxel size of 16 mm with a 75% overlap and a smoothing factor of 1.5 were used.

Using in-house MATLAB code, average and peak jet velocity (U_{jave}, U_{jmax}), jet length to jet diameter ratios (L_v/D_ω, L_ω/D_ω), linear impulse (**I**), and angular impulse (**A**) were calculated. Velocity-based jet length (L_v) is the extent over which the jet centerline velocity magnitude is above a specified threshold (20% of maximum velocity), whereas vorticity-based jet length (L_ω) is the extent over which the jet vorticity field is above a specified threshold (20% of maximum vorticity). The jet diameter (D_ω) is the distance between vorticity cores (regions where vorticity is >90% of peak jet vorticity) perpendicular to the jet centerline.

Linear impulse (**I**) was calculated using:

$$\mathbf{I}/\rho = \frac{1}{2}\int \mathbf{x}\times\boldsymbol{\omega}\mathrm{d}V, \quad (2)$$

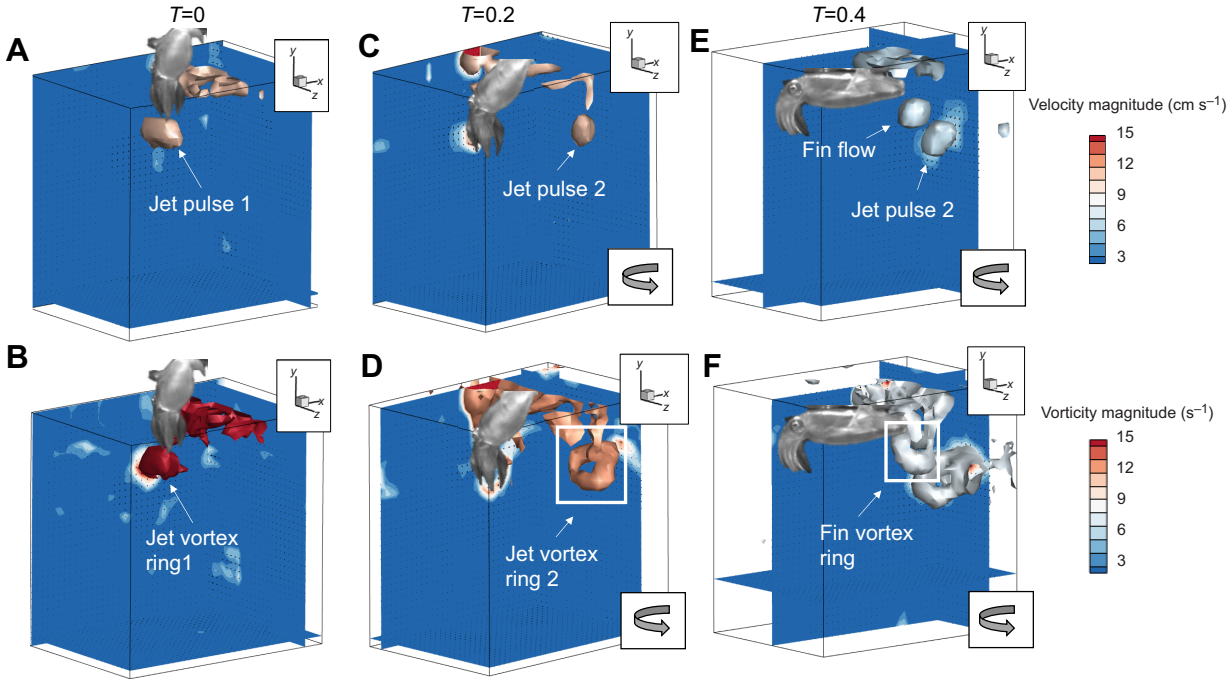

Fig. 3. 3D velocity isosurfaces (top row) and 3D vorticity isosurfaces (bottom row) for a turning sequence. Jet pulse 1 (T=0 s; A,B), which was directed downward, produced an upward motion of the squid, but no turning motion. The turn occurred during the next two frames, with both jet pulse 2 (T=0.2; C,D) and fin flow (T=0.4; E,F) producing the turn. Thus, vorticity from both frames (highlighted by the white rectangles in D and F) was measured to determine impulse and angular impulse. The direction of the turn is shown in the lower right insets in C–F.

where $\mathbf{x}$ is the position vector and $\boldsymbol{\omega}$ is the vorticity vector ($\boldsymbol{\omega}=\nabla\times\mathbf{u}$ where $\mathbf{u}$ is the velocity vector and the partial derivatives were calculated using central differences), ρ is the fluid density, and the integral is computed over the volume of the vortex, V, where the vorticity is non-zero (Saffman, 1992). Similarly, angular impulse ($\mathbf{A}$) was computed from (Wu et al., 2007):

$$\mathbf{A}/\rho = -\frac{1}{2}\int |\mathbf{x}|^2\boldsymbol{\omega}\mathrm{d}V. \quad (3)$$

By default, $\mathbf{A}$ associated with a vortex selected for analysis was computed with respect to the centroid of the vorticity magnitude of the vortex using Eqn 3. $\mathbf{A}$ about the center of mass of the squid was then computed by shifting the origin of the calculated impulse (by shifting the origin of $\mathbf{x}$) to the squid center of mass using the distance between the center of mass of the squid and the centroid of the vortex (determined from the custom MATLAB routines) in accordance with Eqn 3. Angular impulse for the jet, fins and arms was categorized based on the axis of rotation the impulse was acting about, i.e. yaw, roll or pitch. The yaw axis was defined as the major axis of the turn as the squid were primarily turning in the x–z plane. Rotation of the squid in the roll and pitch planes was considered secondary, i.e. these rotations did not occur about the main turning axis.

Angular impulse about the roll axis was computed with the yaw angle (θ_{yaw}), which is the angle of the body relative to the x-axis in the x–z plane (Fig. 2), using the following equation:

$$\mathbf{A}_{roll} = \mathbf{A}_x\cos\theta_{yaw} - \mathbf{A}_z\sin\theta_{yaw}. \quad (4)$$

Angular impulse about the pitch axis was computed using the following equation:

$$\mathbf{A}_{pitch} = \mathbf{A}_z\cos\theta_{yaw} + \mathbf{A}_x\sin\theta_{yaw}. \quad (5)$$

For the jet, fins and arms, $\mathbf{A}_{yaw}$ (main turning axis), $\mathbf{A}_{roll}$ and $\mathbf{A}_{pitch}$ were calculated. For turning sequences where flows from at least two of these systems were captured within the sampling volume, fractional contributions for the systems were determined. As flows from all three systems were not always resolvable, the percentage contribution from each system averaged across all turns does not necessarily add to 100%. For $\mathbf{A}_{yaw}$, contributions were determined using two methods. First, fractional contributions based only on $\mathbf{A}_{yaw}$ that contributed constructively to the main turning motion, i.e. flows of the correct sign to induce the turn, were computed, with flow contributions acting counter to the direction of the turn being assigned a 0% contribution. Second, fractional contributions based on the absolute value of $\mathbf{A}_{yaw}$, i.e. $|\mathbf{A}_{yaw}|$, were determined, with all values being considered irrespective of whether they acted to produce or oppose the turn. For flows around the non-primary axes, fractional contributions from each system were based on $|\mathbf{A}_{roll}|$ and $|\mathbf{A}_{pitch}|$ values, as the objective was to determine general contributions within these secondary planes. Total impulse magnitude (I) for the jet, fins and arms was determined as the magnitude of the impulse vector for the respective system. This metric provided a measure of each system's flow strength.

Statistical analysis

Kinematic variables (Ω_{mean}, Ω_{max}, R/L_{mean}, R/L_{min}, fin frequency, jet frequency, θ_M, θ_L, θ_{DV}) and jet property variables (I, $|\mathbf{A}_{yaw}|$, $|\mathbf{A}_{roll}|$, $|\mathbf{A}_{pitch}|$, U_{jave}, U_{jmax}, L_ω/D_ω, L_v/D_ω) were analyzed using multivariate analysis of variance (MANOVA), a procedure for comparing multivariate sample means, to test for differences in turning orientation, i.e. AF versus TF (SPSS v. 28). One sequence was removed from jet property analyses because jet flow was too close to the sampling boundary. Pillai's Trace statistic was used to assess significance at α=0.05. When significance was detected, subsequent analyses of variance (ANOVA) were performed to determine which variables were significant. Two-factor ANOVA were used to assess the effect of propulsor (jet, fins, arms) and turning orientation (AF, TF) on contributions to impulse and angular impulse, with Fisher's least significant difference (LSD) *post hoc* tests being performed following propulsor significance. Data variables were transformed to meet assumptions of normality, with Shapiro–Wilk tests being used for assessment of normality. Log transformations were used for R/L, Ω, θ_L, fin/jet frequencies, $|\mathbf{A}_{yaw}|$, $|\mathbf{A}_{roll}|$, $|\mathbf{A}_{pitch}|$, L_ω/D_ω, L_v/D_ω; square root transformations were used for θ_M, θ_{DV}, I, U_{jave}, U_{jmax}; and arcsine transformations were used for propulsor percentage contributions. Linear regression analysis was performed on Ω_{mean} versus θ_L, R/L_{mean} versus θ_{DV}, Ω_{mean} versus R/L_{mean}, Ω_{mean} versus U_{jave}, Ω_{max} versus U_{jmax}, Ω_{mean} and Ω_{max} versus $|\mathbf{A}_{yaw}|$, and Ω_{mean} and R/L_{mean} versus L_ω/D_ω. To meet assumptions of normality and homogeneity of variance, R/L and Ω values were log transformed. Untransformed data are presented in figures for ease of interpretation, and all mean values are reported ±s.e.m. unless stated otherwise.

RESULTS

Kinematics

Turns were largely horizontal, with a mean trajectory angle of 6.77±1.20 deg in the x–y plane. For TF turns, the keeled third arm pair often extended away from the remaining arms (Fig. 2A), whereas during AF turns, the arms were frequently positioned in a streamlined, conical arrangement (Fig. 2C). Curving of arms away from the mantle's longitudinal axis, i.e. curling, in the x–z plane (perspective of the dorsal camera) (Fig. 2B,C) and the x–y plane (perspective of lateral camera) (Fig. 2D,F) were common in both AF and TF turning sequences. During banking turns (4% of turns), the body tilted with the fins extended (Fig. 2E), resulting in the production of long streams of vorticity (see below). These turns were broad (R/L=0.26±0.03) and slow (Ω=20.8±6.16 deg s^{-1}). For a few turns, the arms oscillated up and down to push flows and assist the turn. No significant difference in body length was detected for animals performing AF turns (mean±s.d. DML=7.3±0.7 cm; TL=11.2±1.1 cm) and TF turns (DML=7.2±0.8 cm; TL=11.1±1.2 cm) (t-test, P>0.75).

There was a significant difference in kinematic properties based on swimming orientation (MANOVA: $F_{9,58}$=3.10, P=0.004, Pillai's Trace=0.325, partial η^2=0.325). Subsequent ANOVA revealed that θ_{DV} during AF turning (46.3±5.87 deg) was significantly greater than that during TF turning (26.0±3.49 deg) (Fig. 4A), which is indicative of greater levels of AF arm curling in the x–y plane (lateral camera perspective). Follow-up ANOVA also indicated that mean and peak angular velocities were greater for TF turns (Ω_{mean}=81.0±8.50 deg s^{-1}, Ω_{max}=164.2±22.19 deg s^{-1}) than for AF turns (Ω_{mean}=55.1±6.58 deg s^{-1}, Ω_{max}=102.3±9.88 deg s^{-1}) (Fig. 4B,C). The greatest Ω_{max} recorded was 775 deg s^{-1}, which was performed TF. Finally, subsequent ANOVA indicated that R/L_{min} was significantly lower for AF turns (0.0043±0.0011) than for TF turns (0.0079±0.0015) (Fig. 4D). The lowest R/L_{min} detected, which was performed AF, was 9.27×10^{-5}.

No significant differences in the two turning orientations were found for R/L_{mean} (AF=0.162±0.020, TF=0.182±0.022), fin frequency (AF=2.25±0.17 Hz, TF=2.44±0.17 Hz), jet frequency (AF=2.12±0.09 Hz, TF=2.29±0.10 Hz), θ_M (AF=23.61±3.17 deg, TF=25.43±3.15 deg) or θ_L (AF=10.68±3.12 deg, TF=12.05±1.50 deg)

Journal of Experimental Biology (2022) 225, jeb244151. doi:10.1242/jeb.244151

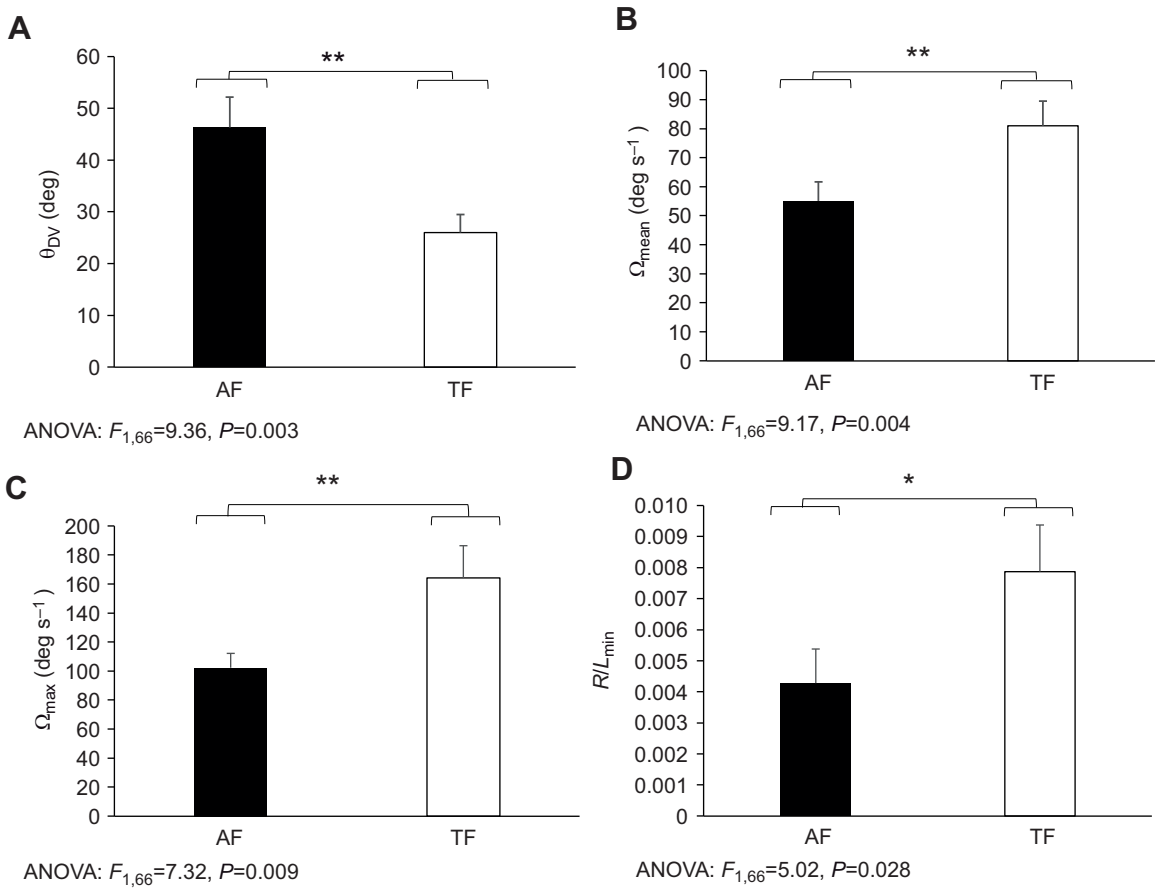

Fig. 4. Kinematic properties based on swimming orientation. Dorsoventral arm angle (θ_{DV}; A), mean angular velocity (Ω_{mean}; B), maximum angular velocity (Ω_{max}; C) and minimum turning radius (R/L_{min}; D) for arms-first (AF) and tail-first (TF) turns. ANOVA performed following a significant MANOVA are depicted. All differences are significant, as indicated with asterisks. Data are means+1 s.e.m.

(P>0.05). Fin frequencies across turns ranged from 0 to 4.8 Hz, with symmetric finning occurring over many of the analyzed sequences. In some cases, asymmetric finning was present, whereby the outboard fin oscillated out of phase or at higher frequency than the inboard fin, often near the end of a turning sequence. The range of jet frequencies was 1.3–4.0 Hz. As θ_{DV} increased, R/L_{mean} decreased; as θ_L increased, Ω_{mean} increased (Fig. 5A,B). No clear relationship between R/L_{mean} and Ω_{mean} was detected (Fig. 5C).

Hydrodynamics

Jet flows ranged from short vortex rings (L_ω/D_ω<3) (AF: Fig. 6A,B; TF: Fig. 7A,B) to longer multi-ringed and tubular jets (L_ω/D_ω=3–5) (Figs 6E,F and 7C,D), and to long jets with both leading-edge vortex ring and trailing jet components (L_ω/D_ω>5) (Figs 7E,F). In general, jet flow signatures were more prominent than fins flows, though fin-induced vortex rings (e.g. Figs 6B,D and 7E) and fin-generated vorticity streams (e.g. Figs 6C and 7B), a defining characteristic of banking turns, were present in some turning sequences. AF turns commonly included pronounced fin undulations with more complex vorticity structures (e.g. Fig. 6F). For some TF turning sequences where the arms oscillated up and down or the third arm pair extended outward, defined thin streams of shed vorticity were observed (e.g. Fig. 7D), but in most sequences, arm flows consisted of disorganized regions of concentrated vorticity.

The pulsed jet produced 67.4±3.1% of I, with the fins and arms contributing 27.3±4.1% and 31.2±3.8%, respectively. ANOVA and LSD *post hoc* tests indicated that the jet contribution to I was greater than that of the fins and arms, but no significant difference between fin and arm contributions was detected (Fig. 8A). Additionally, no significant differences in these contribution percentages between turning orientations was detected (two-factor ANOVA: $F_{1,60}$=0.389, P=0.535), nor was there a significant orientation×propulsor interaction ($F_{2,60}$=2.66, P=0.078). Average y-impulse ($\mathbf{I}_y$) across all turns was negative for the jet, fins and arms. Given the impulse applied to the squid is in the opposite direction by Newton's third law, the negative sign indicates these systems were important for maintaining vertical position in the water column. When considering only angular impulse that contributes constructively to motion along the main turning axis (yaw axis), the pulsed jet produced 71.3±6.7% of $\mathbf{A}_{yaw}$ compared with 28.5±8.0% for the fins and 19.5±9.4% for the arms. As with I, ANOVA and *post hoc* tests revealed that the jet contribution to $\mathbf{A}_{yaw}$ was significantly greater than that of the fins and arms, but fin and arm contributions were not statistically different (Fig. 8B). The contribution percentages did not differ according to orientation, i.e. AF versus TF (two-factor ANOVA: $F_{1,43}$=0.001, P=0.987), nor was the propulsor×orientation interaction significant (two-factor ANOVA: $F_{2,43}$=0.012, P=0.988). When considering absolute values of angular impulse about the main turning axis ($|\mathbf{A}_{yaw}|$), the jet contributed significantly more angular impulse than the other systems, and no difference was detected between fin and arm contributions (Fig. 8C). No significant differences in contribution percentages to $|\mathbf{A}_{yaw}|$ between turning orientations

Journal of Experimental Biology (2022) 225, jeb244151. doi:10.1242/jeb.244151

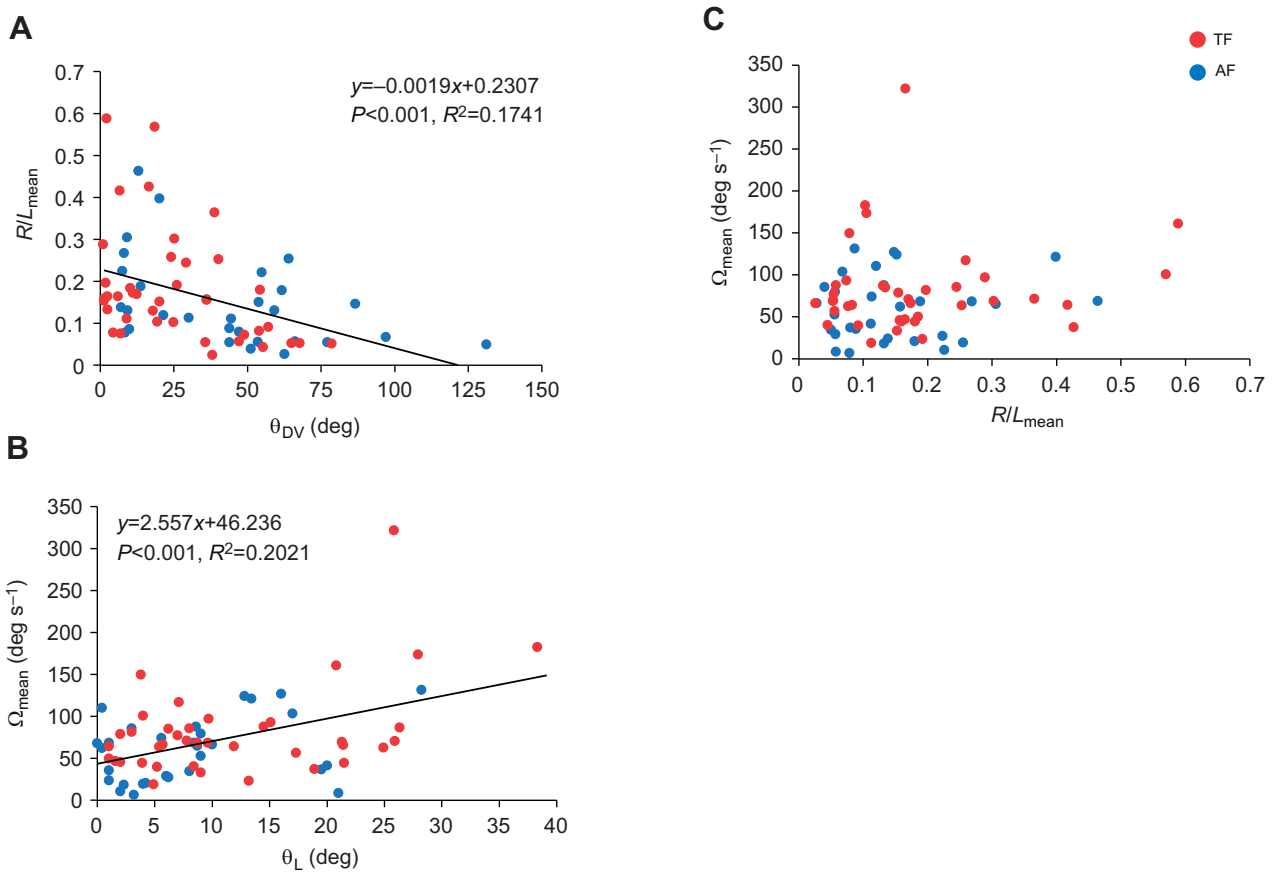

Fig. 5. Relationships between kinematic properties. Linear regression of length-specific turning radius (R/L_{mean}) versus dorsoventral arm angle (θ_{DV}; A), linear regression of mean angular velocity (Ω_{mean}) versus lateral arm angle (θ_L; B), and scatter plot of mean angular velocity (Ω_{mean}) versus length-specific turning radius (R/L_{mean}; C). Red and blue points depict TF and AF turns, respectively. Regressions in A and B are significant; no significant relationship was detected in C.

was detected (two-factor ANOVA: $F_{1,62}$=0.775, P=0.382), nor was there a significant orientation×propulsor interaction ($F_{2,62}$=1.05, P=0.357). Of the turning sequences where flows from multiple propulsors/control surfaces were fully visible in the sampling volume, 27.8% of fin flows and 50% of arm flows acted counter to the direction of the turn, indicating that drag was being produced to slow and/or stabilize the turn along the yaw axis.

The proportion of $|\mathbf{A}_{roll}|$ did not differ according to propulsor (two-factor ANOVA: $F_{2,58}$=1.716, P=0.189) or orientation (ANOVA: $F_{1,58}$=0.233, P=0.631), and the propulsor×orientation interaction was insignificant (ANOVA: $F_{2,58}$=0.571, P=0.568). While not significant, a trend of greater $|\mathbf{A}_{roll}|$ contributions by the jet (52.2±4.9%) compared with the fins (41.4±6.4%) and arms (38.3±7.2%) was apparent (Fig. 8D). The fins acted counter to the jet $\mathbf{A}_{roll}$ in 57.1% of the turns, and of those turns where a strong roll was observed (and fin flows were visible), the fins produced $\mathbf{A}_{roll}$ in the direction of the roll in 83.3% of the sequences compared with 33.3% of the sequences for jet flows. The arms acted counter to the jet $\mathbf{A}_{roll}$ in 30.8% of the turns, and of those turns where a pronounced roll was observed (and arm flows were visible), the arms produced $\mathbf{A}_{roll}$ in the direction of the roll in 37.5% of sequences compared with 75% of the sequences for jet flows. A significant difference in propulsor contributions to $|\mathbf{A}_{pitch}|$ was detected, where the jet contributed 59.7±4.6% of $|\mathbf{A}_{pitch}|$, while the fins and arms contributed 32.1±6.4% and 40.5±6.2%, respectively. ANOVA and LSD *post hoc* tests revealed that the jet contributed significantly more to $|\mathbf{A}_{pitch}|$ than the other systems, but no significant difference between the arms and fins was detected (Fig. 8E). No difference in these contributions according to turn orientation was detected (two-factor ANOVA: $F_{1,58}$=0.003, P=0.958), nor was a significant orientation×propulsor interaction present (two-factor ANOVA: $F_{2,58}$=0.200, P=0.819). The fins acted counter to the jet $\mathbf{A}_{pitch}$ in 19.0% of the turns, and of those turns where a pronounced pitch was observed with visible fin flows, the fins produced $\mathbf{A}_{pitch}$ in the direction of the pitch in 63.2% of the sequences compared with 73.7% of the sequences for jet flows. The arms acted counter to the jet $\mathbf{A}_{pitch}$ in 42.9% of the turns, and of those turns where a pronounced pitch was observed with visible arm flows, the arms produced $\mathbf{A}_{pitch}$ in the direction of the pitch in 64.3% of the sequences compared with 78.6% of the sequences for jet flows.

A significant difference in jet properties based on swimming orientation was detected (MANOVA: $F_{8,58}$=3.186, P=0.005, Pillai's Trace=0.305, partial η^2=0.305). Subsequent ANOVA revealed that jet I,$|\mathbf{A}_{yaw}|$, $|\mathbf{A}_{roll}|$ and $|\mathbf{A}_{pitch}|$ were greater for TF turns (I=5.07×10^{-3}±6.04×10^{-4} kg m s^{-1}, $|\mathbf{A}_{yaw}|$=8.23×10^{-4} ±2.40×10^{-4} kg m^2 s^{-1}, $|\mathbf{A}_{roll}|$=4.24×10^{-4}±6.60×10^{-5} kg m^2 s^{-1}, $|\mathbf{A}_{pitch}|$=5.90×10^{-4}±1.21×10^{-4} kg m^2 s^{-1}) than for AF turns (I=3.24×10^{-3}±3.37×10^{-4} kg m s^{-1}, $|\mathbf{A}_{yaw}|$=2.09×10^{-4}±3.93 ×10^{-5} kg m^2 s^{-1}, $|\mathbf{A}_{roll}|$=1.72×10^{-4}±3.58×10^{-5} kg m^2 s^{-1}, $|\mathbf{A}_{pitch}|$ =2.36×10^{-4}±7.21×10^{-5} kg m^2 s^{-1}) (Fig. 9A–D).

Journal of Experimental Biology (2022) 225, jeb244151. doi:10.1242/jeb.244151

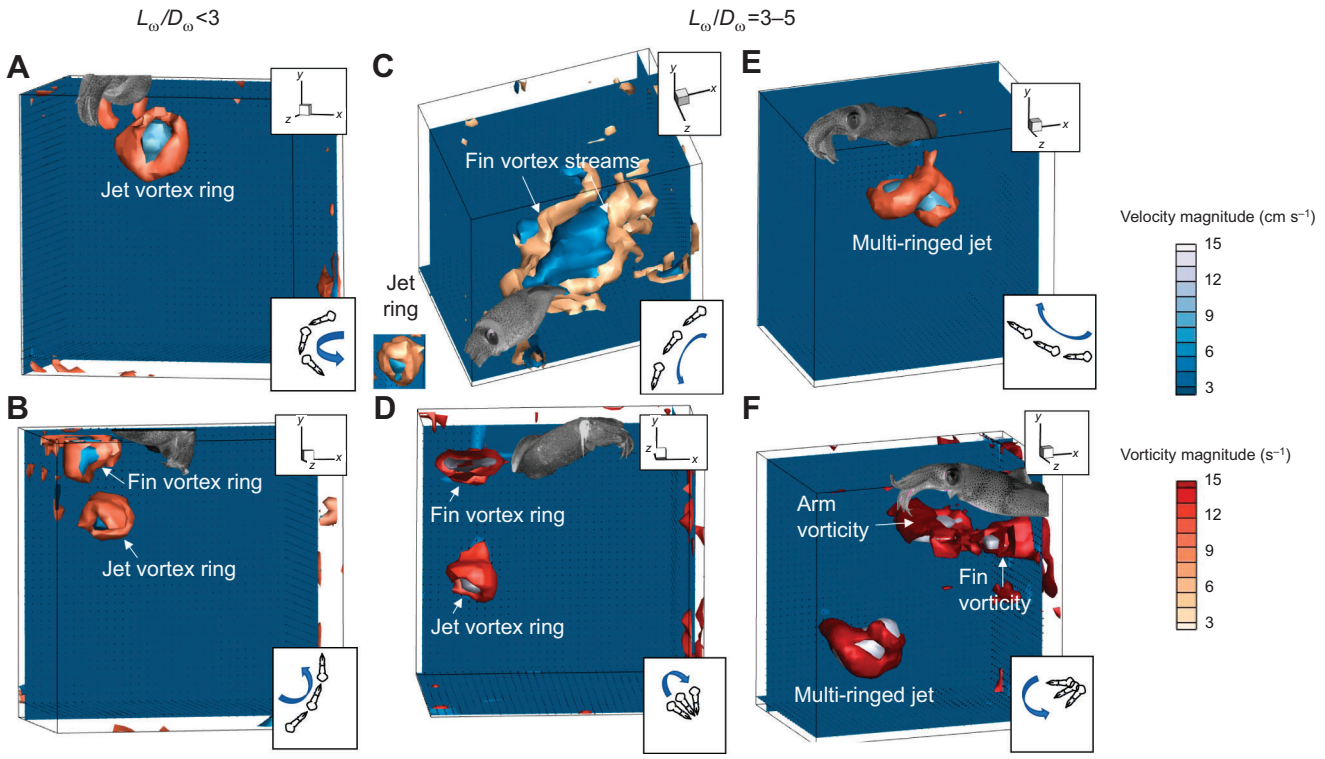

Fig. 6. Velocity isosurfaces (blue gradient) and vorticity isosurfaces (red gradient) for brief squid turning AF. Jets are shown with length to diameter ratios (L_ω/D_ω)<3 (A,B) and L_ω/D_ω=3–5 (C–F). Insets in the lower right corner depict turning paths in the *x*–*z* plane; jet flow below the fin flows is shown in the lower left of C.

Average and maximum jet velocity for TF turns (U_{jave}= 12.45±1.17 cm s^{-1}, U_{jmax}=19.38±1.73 cm s^{-1}) were significantly greater than those for AF turns (U_{jave}=9.15±0.79 cm s^{-1}, U_{jmax}=13.81±1.15 cm s^{-1}) (Fig. 9E,F). Jets were longer during TF turns relative to AF turns, with L_ω/D_ω=3.88±0.25 and L_v/D_ω=4.31±0.27 for TF turns and L_ω/D_ω=2.58±0.17 and L_v/D_ω=3.03±0.17 for AF turns (Fig. 9G,H). Additionally, Ω_{mean} increased with greater U_{jave}, Ω_{max} increased with greater U_{jmax}, and Ω_{mean} and Ω_{max} increased with higher $|\mathbf{A}_{yaw}|$, with TF turns playing an integral role in these relationships (Fig. 10A–D). A strong linear relationship between L_ω/D_ω and Ω_{mean} or L_ω/D_ω and R/L_{mean} was not found (P>0.05) (Fig. 10E,F).

DISCUSSION

Propulsor/control surface contributions to turning

Our results indicate that the pulsed jet is the main driver of turns in the neritic brief squid, *Lolliguncula brevis*, with the fins and arms playing subordinate but important roles for turning performance. Heavy reliance on the pulsed jet for impulse generation and angular impulse about the primary turning axis (yaw axis; >67% of I and $\mathbf{A}_{yaw}$) is not surprising given that jet flows of varying magnitude can be directed in any direction below the animal. While the jet exits through a funnel that is closer to the squid's center of mass than the fins or arms, jet flows are higher in velocity and impulse, and extend farther from the body, allowing the jet to generate greater magnitude forces and higher resultant torque than the other systems. Given higher magnitude force production, most neritic squids also rely more heavily on the jet than on the fins during rectilinear swimming (O'Dor, 1988; Anderson and Grosenbaugh, 2005; Bartol et al., 2001b, 2008, 2016). Not only is the jet the dominant system for effecting turns about the yaw axis but it also contributes significantly more $|\mathbf{A}_{pitch}|$ than the fins and arms, providing on average ∼60% of $|\mathbf{A}_{pitch}|$. A trend in greater contributions of the jet to $|\mathbf{A}_{roll}|$ relative to the other propulsors/control surfaces was also observed. Considering high impulse output and flow directionality associated with the jet, it seems reasonable that the jet would also contribute most to angular impulse in the non-primary axes during turns.

The fins and arms are located far from the center of mass, representing the moment arm extremes along the body axis. As a result of their location and activity levels during most turns, these systems were expected to contribute to turning performance, and many previous studies have alluded to the potential role of fins in torque corrections (Zuev, 1966; Hoar et al., 1994; Bartol et al., 2001b; 2016, 2018; Stewart et al., 2010). Our results support this expectation, with the fins and arms contributing >30% of overall angular impulse about the three axes, i.e. yaw (primary), roll and pitch. The arms and fins provided statistically similar relative impulse, angular impulse about the turning axis, and angular impulse about the non-turning axes. Of these measures, the greatest qualitative difference between the fins and arms occurred along the main turning axis, where the fins contributed 29% of $\mathbf{A}_{yaw}$ to effect the turn versus 20% of $\mathbf{A}_{yaw}$ contributed by the arms. This trend is reasonable given the fins play an important role in rectilinear swimming, contributing on average ∼32–35% of the total thrust (Bartol et al., 2016). The absence of statistically significant differences in arm and fin relative contributions, irrespective of whether they are located at the leading or trailing edge of the squid, underscores the flexibility of the squid system. Having accessory systems to complement the jet and contribute angular impulse facilitates turning trajectory adjustment and control.

An important finding of this study was that the fins and arms sometimes acted counter to the angular impulse generated by the pulsed jet. Specifically, fins and arms provided opposing $\mathbf{A}_{yaw}$

Journal of Experimental Biology (2022) 225, jeb244151. doi:10.1242/jeb.244151

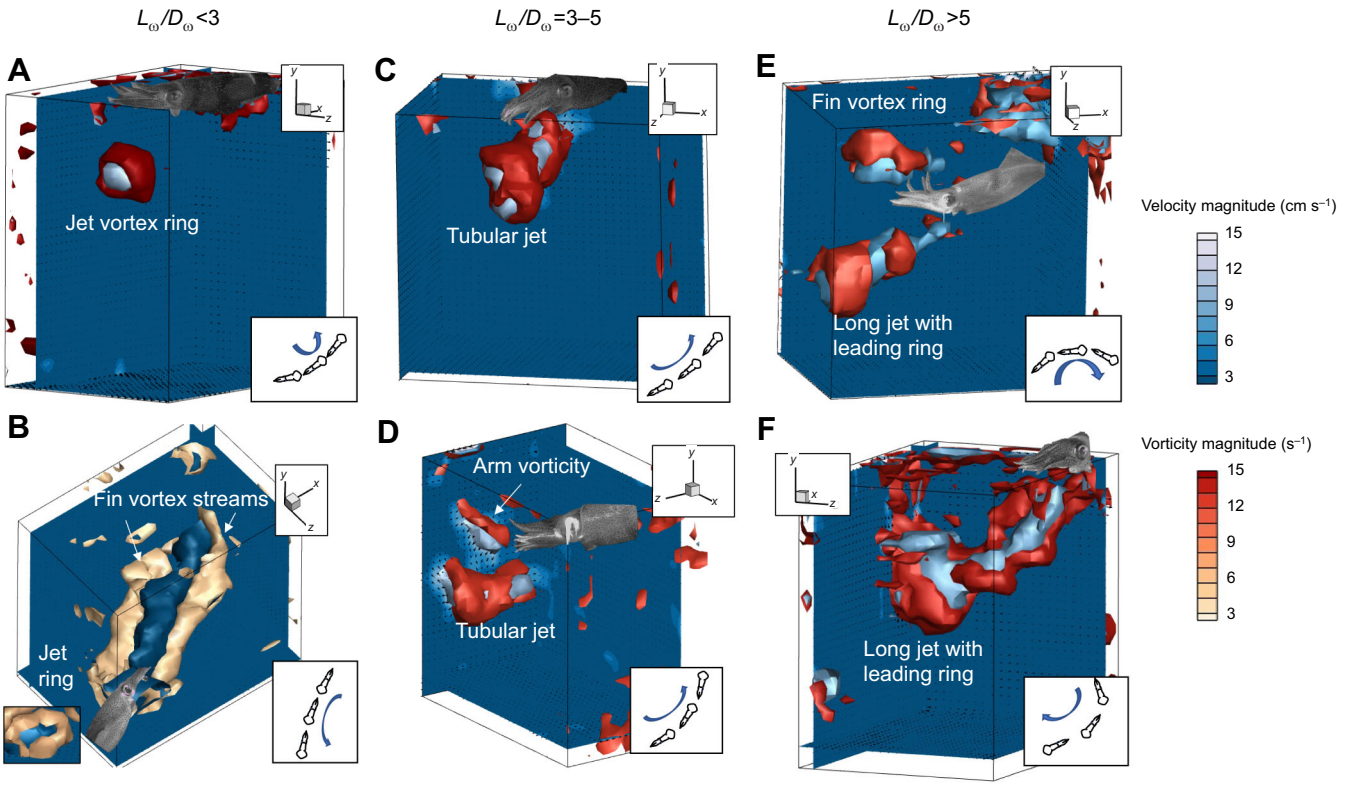

Fig. 7. Velocity isosurfaces (blue gradient) and vorticity isosurfaces (red gradient) for brief squid turning TF. Jets are shown with L_ω/D_ω<3 (A,B), L_ω/D_ω=3–5 (C,D) and L_ω/D_ω>5 (E,F). Insets depict turning paths in the *x*–*z* plane; jet flow below the fin flows is shown in the lower left of B.

(angular impulse about the main turning axis) in ∼28% and ∼50%, respectively, of analyzed turns where flows from the jet and at least one other system were resolvable. These opposing flows were likely important for improving turn authority, as indicated by significantly lower R/L values for sequences with counteracting fin flows in $\mathbf{A}_{yaw}$ (R/L=0.10±0.04) compared with those with aligning fin flows (R/L=0.18±0.02) (*t*-test, P=0.04). For angular impulse along the non-turning axes, the fins and arms provided opposing $\mathbf{A}_{roll}$ in 57% and 31%, respectively, of the turns and opposing $\mathbf{A}_{pitch}$ in 19% and 43%, respectively, of the turns where flows from the jet and at least one other system were resolvable. The reasons for these opposing forces are nuanced, with moment corrections and active perturbation playing varying roles depending on the turning sequence.

Limited roll was observed across most turns, suggesting that counter flows from the fins and arms may have limited roll instabilities produced by the pulsed jet, like the stabilizing function of pectoral and median fins in fishes (Hove et al., 2001; Webb, 2006). Banked turns where the fins were extended and streams of trailing vorticity were observed (Figs 6C and 7B) are the notable exception where significant roll was observed. During these turns, the squid jetted, lowered the inboard fin ventrally, and extended the outboard fin dorsally to induce a roll, which was followed by a banked gliding period. This behavior is similar to banking maneuvers observed in marine mammals, birds, and fishes that lack a dorsal keel (Fish, 2002; Weihs, 1993; Parson et al., 2011; Godfrey, 1985; Hui, 1985), only the banking maneuver is powered by a pulsed jet. When banking, the body and outboard fin are canted at a higher angle incident to the flow, which provides a greater projected area facing the axis of the turn and ultimately greater centripetal force to turn the animal. These turns, which were observed in both the AF and TF orientations, involved high fin lift and roll production (>70% to overall $|\mathbf{A}_{roll}|$) and high angular impulse production from a short, pulsed jet.

Pitching motions were more conspicuous than rolling, with the most pronounced pitch motions involving $\mathbf{A}_{pitch}$ contributions from the jet and fins in the direction of the pitch, resulting in upward movement of the squid's leading edge. On rarer occasions, the arms contributed $\mathbf{A}_{pitch}$ through a pronounced oscillation. Many of these pitch motions moved the leading edge closer to the water surface, a preferred position in some of the experimental runs. The arms played a particularly important role in resisting pitching motions from the jet, offering counter $\mathbf{A}_{pitch}$ flows in 43% of turns (compared with 19% for fins) and contributing qualitatively more $|\mathbf{A}_{pitch}|$ than the fins (41% versus 32%).

The jet, fins and arms all produced impulse to counteract negative buoyancy. Like many neritic squids, brief squid are negatively buoyant (Bartol et al., 2001a,b). To prevent sinking and maintain position in the water column, they need to provide upward-directed forces. Upward impulse generation is especially important when these animals swim and turn at low speeds and dynamic lift forces are minimal (Bartol et al., 2001a,b, 2009a). As swimming speed increases, the vertical component of the jet decreases as a result of a quadratic increase in dynamic lift with speed. Our results indicate that all three systems share the load in lift production through active and passive mechanisms, including downward-directed jet and fin flows and lift generation through highly keeled arm elements.

Turning orientation

Although squids can turn both AF (forward) and TF (backward), TF turning in *L. brevis* was associated with higher angular velocities through the production of longer, faster, more powerful jets than those observed in AF turns. Indeed, agility measures (i.e. Ω_{mean},

Journal of Experimental Biology (2022) 225, jeb244151. doi:10.1242/jeb.244151

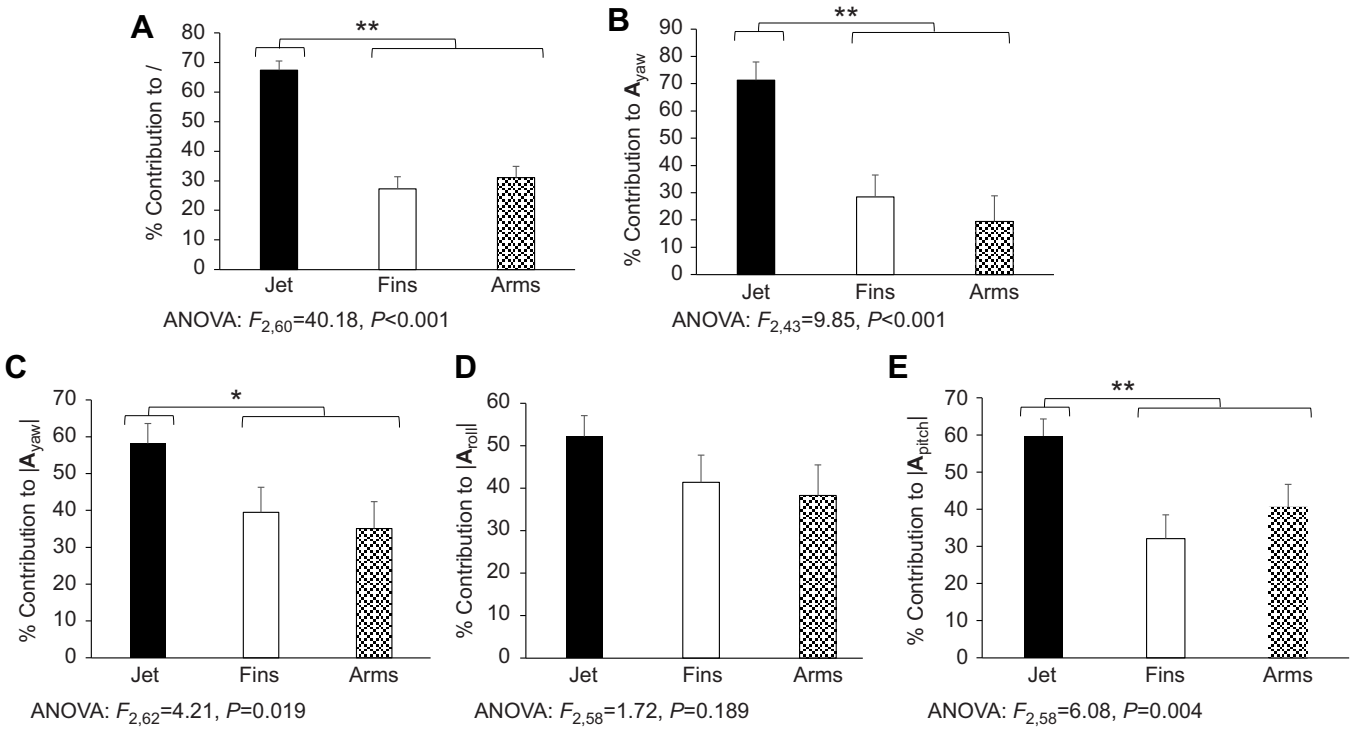

Fig. 8. Jet, fin and arm contributions to impulse magnitude and angular impulse. Percentage contribution of propulsors/control surfaces to impulse magnitude (I; A), constructive angular impulse about the main turning axis ($\mathbf{A}_{yaw}$; B), and absolute angular impulse about the yaw axis ($|\mathbf{A}_{yaw}|$; C), roll axis ($|\mathbf{A}_{roll}|$; D) and pitch axis ($|\mathbf{A}_{pitch}|$; E). ANOVA results are included below each graph, and significance from LSD *post hoc* tests is depicted with asterisks. Data are means+1 s.e.m.

Ω_{max}), jet impulse metrics (I, $|\mathbf{A}_{yaw}|$, $|\mathbf{A}_{roll}|$, $|\mathbf{A}_{pitch}|$) and jet property measurements (U_{jave}, U_{jmax}, L_{ω}/D_{ω}, L_{v}/D_{ω}) were all significantly greater for TF turns than for AF turns. These differences may derive from muscle constraints of the funnel. When turning in the AF orientation, the funnel bends to direct jet flows rearward, which is unnecessary during TF turning. To maintain the curved position, the radial muscles of the funnel must shorten to prevent kinking and aperture closure, and ventral longitudinal muscles must contract to maintain funnel arching (Kier and Thompson, 2003). Force limitations of the radial and longitudinal muscles may limit jet impulse, velocity and period, which is consistent with lower reported swimming speed ranges for AF versus TF swimming (Bartol et al., 2001b, 2009a, 2016). As with steady swimming in *L. brevis* (Bartol et al., 2018), we found no difference in fin or jet frequencies or mantle angle between AF and TF orientations during turning sequences. The high angular velocities, impulses and jet velocities observed in TF turns are important for predator evasion, as most escape behaviors are performed TF (Packard, 1969; York and Bartol, 2016; Young, 1938). The TF mode is also preferred for high-speed cruising and schooling/shoaling (Bartol et al., 2001b; 2016; Gosline and DeMont, 1985; O'Dor, 1988; Hurley, 1978; Mather and O'Dor, 1984; Hanlon and Messenger, 2018; Sugimoto et al., 2013). Under these conditions, rapid and powerful course corrections are important to avoid oncoming predators or maintain positioning in the group.

In contrast to TF turns, AF turns were slower and powered by shorter, lower velocity, less powerful jets. These short jet pulses are effective at providing small corrective motions and the capacity for greater dexterity throughout the turn, albeit at low angular velocity, as the angle of the body relative to flow changes constantly. Using this approach, squid turning AF were able to achieve significantly lower R/L_{min}. Although a significant difference in R/L_{mean} was not detected, a trend in lower values for AF turns (R/L_{mean}=0.16) versus TF turns (R/L_{mean}=0.18) was present. Higher R/L_{min} and R/L_{mean} for TF swimming make sense because longer, high force pulses result in less control of the turning path and greater translation, requiring more effort to steer into a turn. The ability to turn precisely in an AF orientation is useful for navigating complex environments, positioning relative to and striking prey, mating and antagonistic encounters (Bartol et al., 2001b; Hanlon and Messenger, 2018; Jastrebsky et al., 2016).

As mentioned above, arm and fin contributions to effecting and stabilizing turns are somewhat interchangeable. However, the two systems operate differently depending on turning orientation. During TF turns, a single vortex ring (e.g. Fig. 7E) was often associated with each downstroke, similar to fin mode I reported in Stewart et al. (2010). During AF turns, the fins generally exhibited more undulatory motions with resulting linked regions of vorticity (e.g. Fig. 6F), similar to fin mode II_A observed in Stewart et al. (2010), only the flows were not as downwardly directed. A greater horizontal flow component may be related to the need to direct impulse toward the COR for turning, creating the centripetal impulse necessary to complete the turn (Fish et al., 2003; Parson et al., 2011). The prevalence of linked vortices and fin wave motions recorded in AF turns is consistent with fin wake and kinematic findings for steady AF swimming (Bartol et al., 2001b, 2009a, 2016, 2018; Stewart et al., 2010).

Arm behavior and mechanics also differed with orientation. When turning AF, squid brought their arms together into a conical arrangement and then curved them laterally in the direction of the turn and/or dorsoventrally. These arm curling behaviors contributed to increased Ω and decreased R/L (see Fig. 5). Both lateral and dorsoventral arm curling were also observed in TF turns, although θ_{DV} was significantly less than in AF turns. A unique characteristic

Journal of Experimental Biology (2022) 225, jeb244151. doi:10.1242/jeb.244151

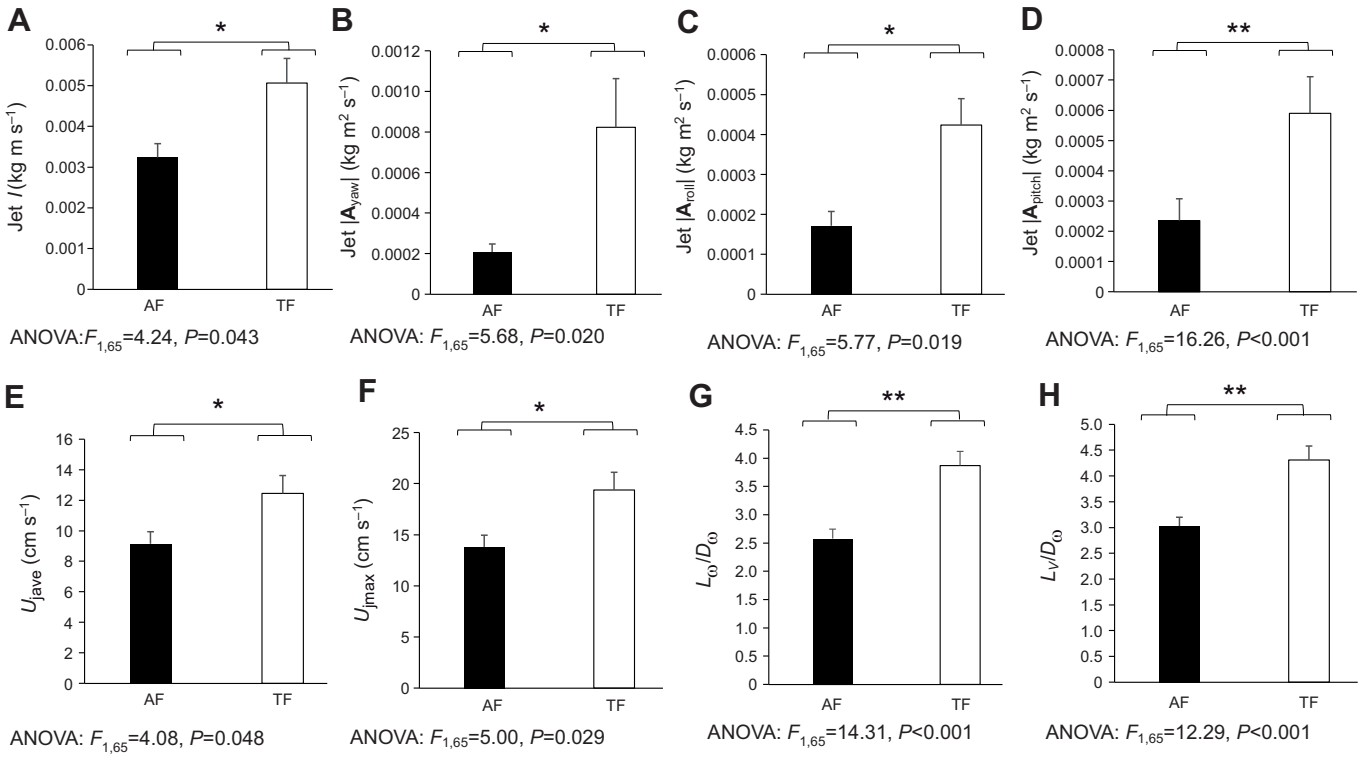

Fig. 9. Jet properties based on swimming orientation. Jet impulse magnitude (I; A), jet absolute angular impulse about the yaw ($|\mathbf{A}_{yaw}|$; B), roll ($|\mathbf{A}_{roll}|$; C) and pitch ($|\mathbf{A}_{pitch}|$; D) axes, mean (U_{jave}; E) and peak (U_{jmax}; F) jet velocity, and jet length to diameter ratios (L_ω/D_ω, G; L_ν/D_ω, H) for AF turns and TF turns. Results from ANOVA performed following a significant MANOVA are shown below bar graphs, with asterisks indicating significance. Data are means+1 s.e.m.

of TF turns was the frequent outward extension of the keeled third arm pair (see Fig. 2A). Together with the posterior positioning of the arm complex, keeled arm extension contributed to qualitatively more $|\mathbf{A}_{yaw}|$ (41% of overall yaw) and $|\mathbf{A}_{roll}|$ (47% of overall roll) compared with AF turns (13% and 30% of overall yaw and roll, respectively). Therefore, dynamic trim control, whereby arms located posteriorly act as biofoils/rudders, appears to be important for turning, similar to the role played by control surfaces located behind the center of mass in other aquatic nekton (Fish, 2002; Webb, 2006).

Hydrodynamic jet flow properties and their relationship to turning performance

Considering the jet is the primary driver of turning performance, we investigated some of the bulk wake properties of this important propulsor, with the goal of determining whether certain jet properties are predictive of turning performance. One potentially relevant metric is the length to diameter ratio (L/D) of the jet. In mechanical studies of pulsed jet flows in stationary water, a physical limit to the size of a vortex ring occurs when the length of the ejected plug of jet flow (L) to the diameter of the jet aperture (D) is ∼4 (Gharib et al., 1998). This physical limit is known as the formation number (F). For jet pulses with $L/D>F$, the vortex ring stops entraining circulation, impulse and energy, and separates, resulting in additional flow forming a trailing jet. In contrast, jet pulses with $L/D<F$ form isolated vortex rings. As L/D approaches F, an optimum in per-pulse-averaged thrust is realized (Krueger and Gharib, 2003), and some have even hypothesized that F is a unifying principle for biological jet propulsion (Dabiri, 2009, 2019). Bartol et al. (2009a, 2016) found both patterns of jet flow occur in squid, i.e. short, isolated vortex rings (jet mode I) and longer jets with leading-edge vortex ring elements followed by a trail of vorticity (jet mode II). Similar modes have been identified in hydromedusa (Katija et al., 2015), and vortex rings (jet mode I) are common in other jet-propelled animals (Sutherland and Madin, 2010; Gemmell et al., 2015, 2021; Costello et al., 2019, 2021). Because identifying the length of the ejected plug of fluid and diameter of the aperture during jet expulsion are challenging in actively swimming animals, Bartol et al. (2009a) introduced the idea of wake-derived L/D measurements, including L_ω/D_ω where F is ∼3. In the present study, we considered both L_ω/D_ω and another wake-based measure, L_ν/D_ω, where F is ∼3.5–4.0.

During turning sequences, mean L_ω/D_ω and L_ν/D_ω were 3.3 and 3.7, respectively. Both means are close to F, with many of the observed jet pulses falling near the transition between short vortex ring jets and longer jets with trailing components. Using short jet pulses for turns confers two significant advantages. First, short pulses provide more controlled impulse than longer jets, acting over specific periods throughout the turning sequence. Second, shorter jet pulses have higher propulsive efficiency for rectilinear swimming (Bartol et al., 2009a, 2016), facilitating potentially better energy use while turning. While short jet pulses ($L_\omega/D_\omega \leq 3$) were common in the wake of turning squid (51% of jets), particularly during AF turns, longer jets ($L_\omega/D_\omega>3$) were also observed (49% of jets). Longer jets can provide high force output, as is the case for steady swimming (Bartol et al., 2009a), resulting in higher impulse and presumably faster angular velocities.

Given the importance of L/D for vortex ring formation, propulsive performance and thrust augmentation (Gharib et al., 1998; Krueger and Gharib, 2003; Bartol et al., 2009a), we expected

Journal of Experimental Biology (2022) 225, jeb244151. doi:10.1242/jeb.244151

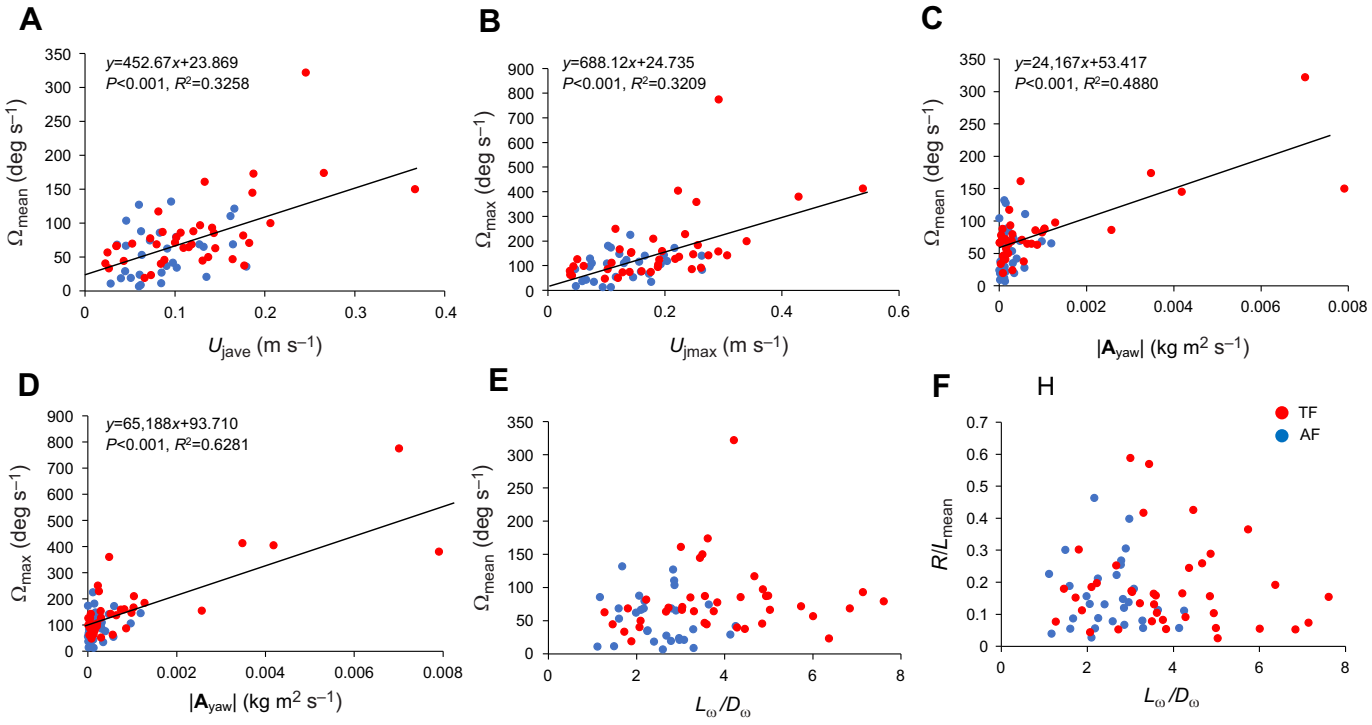

Fig. 10. Relationships of jet properties with kinematic parameters. Mean angular velocity (Ω_{mean}) versus mean jet velocity (U_{jave}; A), peak angular velocity (Ω_{max}) versus peak jet velocity (U_{jmax}; B), Ω_{mean} versus jet absolute angular impulse along the main turning axis ($|\mathbf{A}_{yaw}|$; C), Ω_{max} versus $|\mathbf{A}_{yaw}|$ (D), Ω_{mean} versus jet length to diameter ratio (L_ω/D_ω; E) and mean turning radius (R/L_{mean}) versus L_ω/D_ω (F). Linear regressions shown in A–D are all significant; red and blue points represent TF and AF turning orientations, respectively.

L_ω/D_ω to be linked to R/L and Ω. The absence of a clear relationship between L_ω/D_ω and either R/L_{mean} or Ω_{mean} in this study reflects the versatility of the squid system. Not only can squid control L_ω/D_ω but they can also modulate jet velocity. The five squid with the highest Ω_{mean} produced jets with intermediate L_ω/D_ω (mean 3.5±0.2) and high U_{jave} (23.9±3.9 cm s^{-1}) and U_{jmax} (34.6±5.9 cm s^{-1}) when compared with mean jet velocities for all turning sequences (U_{jave}=10.7±0.8 cm s^{-1}, U_{jmax}=16.5±1.1 cm s^{-1}). Similarly, the five squid with the highest R/L_{mean} produced jets with intermediate L_ω/D_ω (mean 3.3±0.4) and high U_{jave} (17.3±1.2 cm s^{-1}) and U_{jmax} (27.3±2.0 cm s^{-1}). Therefore, in addition to L/D, jet velocity is a factor to consider when evaluating turning performance. Squid can also actively control funnel diameter and the intensity of mantle contractions during jetting, allowing them to produce variants of jet mode I and II, further complicating performance relationships with L/D.

Although a strong relationship between L_ω/D_ω and R/L or Ω was not observed, some jet properties were linked to Ω, and L_ω/D_ω was predictive of other aspects of turn behavior. For example, greater U_{jave}, U_{jmax} and jet $\mathbf{A}_{yaw}$ led to higher angular velocities (Ω), which is reasonable considering the importance of the jet to turns relative to the other systems. As mentioned previously, AF turns were associated with lower L_ω/D_ω than TF turns, with isolated vortex rings being more common. L_ω/D_ω was also important for predicting flow features in the wake of turning squid. When L_ω/D_ω was <3, jet flow rolled up into well-defined vortex ring flows, a pattern observed in both AF and TF turning sequences (Figs 6 and 7) as well as in rectilinear swimming (Bartol et al., 2009a,b). As L_ω/D_ω exceeded 3, both multi-ringed and tubular vorticity structures emerged (see Figs 6 and 7). Although variants of jet mode I and II have also been observed in *L. brevis* during steady swimming (Bartol et al., 2016), deviation from the primary jet modes was more widespread during turning. Jellyfish turns also involve significant deviation from the vortex dynamics of rectilinear swimming, with kinematic modulation of the bell margin during maneuvers resulting in distorted, linked vortex rings that produce large net torque (Gemmell et al., 2015; Dabiri et al., 2020). Our observed deviations are likely a product of the squid using greater mantle and funnel adjustments during turns than during rectilinear swimming. For example, the funnel angle was often modified during jet expulsion while the squid turned, which is rarer in rectilinear swimming, where the funnel is more aligned with the main body axis. At the highest L_ω/D_ω where values were >5 (TF turns), leading edge vortex rings with long trailing jets were observed (Fig. 7). The highest L_ω/D_ω for AF turns was 4.24, so long trailing jet components were absent from AF turns, which is consistent with patterns observed in rectilinear swimming (Bartol et al., 2016).

Angular velocity, turning radius and the arms

A strong relationship between Ω and R/L was not found, which was unexpected given controlling the tightness of a turn should become increasingly more challenging as turns become faster and inertia increases. Jastrebsky et al. (2016), who studied turning kinematics of *L. brevis* without flow analyses, also did not find a strong correlation between Ω and R/L, although a significant relationship between these metrics was observed in the colonial siphonophore *Nanomia bijuga* (Sutherland et al., 2019). Thus, with the use of multiple propulsors and control surfaces, *L. brevis* has the capacity to turn both quickly and tightly when needed. Based on our results, arm positioning is related to Ω and R/L. As θ_L increased and the arms trailed away from the turn (TF) or turned into the turn (AF), Ω_{mean} increased. This trend is consistent with reduced moment of inertia of the body and lower hydrodynamic rotational resistance

when the arms bend this way. As the arms were angled more vertically (greater θ_{DV}), lower R/L_{mean} was observed. This may occur because the vertically oriented arms anchor the pivot point, similar to when a kayaker positions their paddle vertically to turn more tightly. As mentioned previously, vertical arm positioning was especially important for AF turns, where arm curling underneath, or less commonly above, the squid was significantly greater than arm curling in TF turns. Higher levels of arm curling together with short-pulsed jets likely contributed to the lower R/L_{min} observed during AF turns.

The angular velocities and length-specific turning radii reported in the present study differ somewhat from those reported in prior kinematic studies of *L. brevis*. Jastrebsky et al. (2016), who studied turning kinematics using high-speed video, reported R/L_{mean}=0.009, R/L_{min}=0.003, Ω_{mean}=110.3 deg s^{-1} and Ω_{max}=268.4 deg s^{-1}. Our length-specific turning radii were higher and angular velocities were lower, with R/L_{mean}=0.173, R/L_{min}=0.006, Ω_{mean}=70.0 deg s^{-1} and Ω_{max}=137.8 deg s^{-1}. However, when squid approach prey, many of these turning metrics are similar to those reported in the present study, with R/L_{mean}=0.3–0.6, R/L_{min}=0.007–0.01, Ω_{mean}=36–50 deg s^{-1} and Ω_{max}=288–303 deg s^{-1} (Jastrebsky et al., 2017). Additionally, when considering the extremes of performance, squid in the current study slightly outperformed squid in Jastrebsky et al. (2016); the lowest R/L_{min} and highest Ω_{max} were 9.27×10^{-5} and 775 deg s^{-1}, respectively, versus 4.2×10^{-4} and 725.8 deg s^{-1} in Jastrebsky et al. (2016). These measures at the performance extremes also exceed that of the colonial siphonophore *N. bijuga*, which has absolute R/L_{min}=0.05 and Ω_{max}=363 deg s^{-1} (Sutherland et al., 2019). However, when mean values are considered, *N. bijuga*, which generates multiple jets from nectophores, slightly outperforms the *L. brevis* measured in the present study, with R/L_{mean}=0.15, Ω_{mean}=104 deg s^{-1} and Ω_{max}=215 deg s^{-1} (Sutherland et al., 2019). The higher Ω observed in *N. bijuga* may relate to greater jet velocities (peak ∼1.26 m s^{-1}) relative to those considered in the present study (peak ∼0.54 m s^{-1}). When compared with those of other taxa, our recorded agility values place squid at or just below a line separating flexible and hard-bodied animals (see fig. 7 in Fish et al., 2018), which is reasonable for an animal with both rigid and flexible components.

The role of the arms in squid locomotion has received little attention. Based on the results here, the arms are important control surfaces and can serve on occasion as propulsors. During turning sequences, the arms were active, with movements that included lateral/dorsoventral curling to reduce inertial resistance, extension of keeled arm elements, and even active oscillation of the arm complex. Extendable arm keels have been noted in decapod cephalopods (Nichols, 1905; Ishikawa, 1929; Roper, 1964, 1968), and many researchers have hypothesized that the tapered keels, which consist of non-fibrous and fibrous connective tissues plus extensor and retractor muscle fibers, provide lift and stability (Kier, 1982; Bartol et al., 2001b; Hanlon and Messenger, 2018; Nesis, 1987). Results from the current study support this hypothesis. When the keeled arm pair was extended and positioned apart from the other arms, thin vortex streams were produced that provided vertically directed impulse and angular impulse for pitch and roll control (e.g. Fig. 7D). When arm oscillations were used, the resultant flows, which were more disorganized than jet or fin flows, contributed to angular impulse to effect the turn (e.g. Fig. 6F). Although arm curling was common, flows associated with these behaviors were often difficult to resolve because they were obscured by the body or subsumed in the background flow noise. Despite flow quantification limitations, the observed relationships between arm angle and Ω and arm angle and R/L highlight the importance of arm movements for turning performance.

Conclusion

In brief squid, the pulsed jet provided the most angular impulse along the primary (yaw) and non-primary (pitch and roll) axes, with the fins and arms playing subordinate but important roles in providing angular impulse to effect or slow the turn, flows to stabilize or further perturbate pitch and roll, impulse to counteract negative buoyancy, and movements to reduce inertial and hydrodynamic resistance. Because of a flexible funnel capable of vectoring jet flows, squids can easily turn in a forward (AF) and backward (TF) orientation, but our results demonstrate important differences in the two turning orientations. TF turns were powered by long, powerful jets that produced high angular velocities, whereas AF turns were powered by shorter, less powerful jets that produced shorter minimum turning radii. Powerful jets and high angular velocities are important for TF turns employed during escape, cruising and shoaling/schooling where high agility is needed. More controlled, pulsed jets are integral for AF turns used for navigating complex environments, mating, antagonistic encounters and capturing prey where high maneuverability is valued. In contrast to our hypothesis, jet L/D was not a strong predictor of turning radii or angular velocity, though it can be a useful metric for characterizing flow features.

Acknowledgements

We thank Sean Fate and the staff at the Virginia Institute of Marine Science's Eastern Shore Laboratory for assistance during animal capture, and the undergraduate research assistants Eric Amrhein, Jason Dunphy and Tiffany Burkard for assistance during data processing.

Competing interests

The authors declare no competing or financial interests.

Author contributions

Conceptualization: I.K.B., P.S.K., J.T.T.; Methodology: I.K.B., P.S.K.; Software: I.K.B., P.S.K.; Validation: I.K.B., P.S.K.; Formal analysis: I.K.B.; Investigation: I.K.B., A.M.G., A.N.T.; Resources: I.K.B.; Data curation: I.K.B., A.M.G.; Writing - original draft: I.K.B.; Writing - review & editing: A.M.G., A.N.T., P.S.K., J.T.T.; Visualization: I.K.B.; Supervision: I.K.B.; Project administration: I.K.B.; Funding acquisition: I.K.B., P.S.K., J.T.T.

Funding

This project was supported by the National Science Foundation (IOS 1557669, 1557698 and 1557838 to I.K.B., P.S.K. and J.T.T.).

References

Anderson, E. and DeMont, M. E. (2005). The locomotory function of the fins in the squid *Loligo pealei*. *Mar. Freshw. Beh. Phys.* **38**, 169-189. doi:10.1080/10236240500230765

Anderson, E. J. and Grosenbaugh, M. A. (2005). Jet flow in steadily swimming adult squid. *J. Exp. Biol.* **208**, 1125-1146. doi:10.1242/jeb.01507

Bartol, I. K., Mann, R. and Patterson, M. R. (2001a). Aerobic respiratory costs of swimming in the negatively buoyant brief squid *Lolliguncula brevis*. *J. Exp. Biol.* **204**, 3639-3653. doi:10.1242/jeb.204.21.3639

Bartol, I. K., Patterson, M. R. and Mann, R. (2001b). Swimming mechanics and behavior of the shallow-water brief squid *Lolliguncula brevis*. *J. Exp. Biol.* **204**, 3655-3682. doi:10.1242/jeb.204.21.3655

Bartol, I. K., Krueger, P. S., Thompson, J. T. and Stewart, W. J. (2008). Swimming dynamics and propulsive efficiency of squids throughout ontogeny. *Int. Comp. Biol.* **48**, 720-733. doi:10.1093/icb/icn043

Bartol, I. K., Krueger, P. S., Stewart, W. J. and Thompson, J. T. (2009a). Hydrodynamics of pulsed jetting in juvenile and adult brief squid *Lolliguncula brevis*: evidence of multiple jet modes' and their implications for propulsive efficiency. *J. Exp. Biol.* **212**, 1889-1903. doi:10.1242/jeb.027771

Bartol, I. K., Krueger, P. S., Stewart, W. J. and Thompson, J. T. (2009b). Pulsed jet dynamics of squid hatchlings at intermediate Reynolds numbers. *J. Exp. Biol.* **212**, 1506-1518. doi:10.1242/jeb.026948

Bartol, I. K., Krueger, P. S., Jastrebsky, R. A., Williams, S. and Thompson, J. T. (2016). Volumetric flow imaging reveals the importance of vortex ring formation in squid swimming tail-first and arms-first. *J. Exp. Biol.* **219**, 392-403.
Bartol, I. K., Krueger, P. S., York, C. A. and Thompson, J. T. (2018). New approaches for assessing squid fin motions: coupling proper orthogonal decomposition with volumetric particle tracking velocimetry. *J. Exp. Biol.* **221**, jeb176750. doi:10.1242/jeb.176750
Boisclair, D. and Tang, M. (1993). Empirical analysis of the swimming pattern on the net energetic costs of swimming in fishes. *J. Fish Biol.* **42**, 169-183. doi:10.1111/j.1095-8649.1993.tb00319.x
Clifton, G. T. and Biewener, A. A. (2018). Foot-propelled swimming kinematics and turning strategies in common loons. *J. Exp. Biol.* **221**, jeb168831. doi:10.1242/jeb.168831
Costello, J. H., Colin, S. P., Gemmell, B. J. and Dabiri, J. O. (2019). Hydrodynamics of vortex generation during bell contraction by the hydromedusa *Eutonina indicans* (Romanes, 1876). *Biomimetics,* **4**, 44. doi:10.3390/biomimetics4030044
Costello, J. H., Colin, S. P., Dabiri, J. O., Gemmell, B. J., Lucas, K. N. and Sutherland, K. R. (2021). The hydrodynamics of jellyfish swimming. *Ann. Rev. Mar. Sci.* **13**, 375-396. doi:10.1146/annurev-marine-031120-091442
Couch, L. D. and Krueger, P. S. (2011). Experimental investigation of vortex rings impinging on inclined surfaces. *Exp. Fluids,* **51**, 1123-1138. doi:10.1007/s00348-011-1135-x
Dabiri, J. O. (2009). Optimal vortex formation as a unifying principle in biological propulsion. *Ann. Rev. Fluid Mech.* **41**, 17-33. doi:10.1146/annurev.fluid.010908.165232
Dabiri, J. O. (2019). Landmarks and frontiers in biological fluid dynamics. *Phys. Rev. Fluids* **4**, 110501. doi:10.1103/PhysRevFluids.4.110501
Dabiri, J. O., Colin, S. P., Gemmell, B. J., Lucas, K. N., Leftwich, M. C. and Costello, J. H. (2020). Jellyfish and fish solve the challenges of turning dynamics similarly to achieve high maneuverability. *Fluids* **5**, 106. doi:10.3390/fluids5030106
Domenici, P. and Blake, R. W. (1997). The kinematics and performance of fish fast-start swimming. *J. Exp. Biol.* **200**, 1165-1178. doi:10.1242/jeb.200.8.1165
Drucker, E. and Lauder, G. (2001). Wake dynamics and fluid forces of turning maneuvers in sunfish. *J. Exp. Biol.* **204**, 431-442. doi:10.1242/jeb.204.3.431
Drucker, E. G. and Lauder, G. V. (2003). Function of pectoral fins in rainbow trout: behavioral repertoire and hydrodynamic forces. *J. Exp. Biol.* **206**, 813-826. doi:10.1242/jeb.00139
Ehlinger, T. J. and Wilson, D. S. (1988). Complex foraging polymorphism in bluegill sunfish. *Proc. Natl. Acad. Sci.* **85**, 1878-1882. doi:10.1073/pnas.85.6.1878
Fish, F. E. (2002). Balancing requirements for stability and maneuverability in cetaceans. *Integr. Comp. Biol.* **42**, 85-93. doi:10.1093/icb/42.1.85
Fish, F. E., Hurley, J. and Costa, D. P. (2003). Maneuverability by the sea lion *Zalophus californianus*: turning performance of an unstable body design. *J. Exp. Biol.* **206**, 667-674. doi:10.1242/jeb.00144
Fish, F. E., Kolpas, A., Crossett, A., Dudas, M. A., Moored, K. W. and Bart-Smith, H. (2018). Kinematics of swimming of the manta ray: three-dimensional analysis of open-water maneuverability. *J. Exp. Biol.* **221**, jeb166041. doi:10.1242/jeb.166041
Gemmell, B. J., Troolin, D. R., Costello, J. H., Colin, S. P. and Satterlie, R. A. (2015). Control of vortex rings for maneuverability. *J. Roy. Soc. Interface* **12**, 20150389. doi:10.1098/rsif.2015.0389
Gemmell, B. J., Dabiri, J. O., Colin, S. P., Costello, J. H., Townsend, J. P. and Sutherland, K. R. (2021). Cool your jets: biological jet propulsion in marine invertebrates. *J. Exp. Biol.* **224**, jeb222083. doi:10.1242/jeb.222083
Gharib, M., Rambod, E. and Shariff, K. (1998). A universal time scale for vortex ring formation. *J. Fluid Mech.* **360**, 121-140. doi:10.1017/S0022112097008410
Gharib, M., Pereira, F., Dabiri, D., Hove, J. R. and Modarress, D. (2002). Quantitative flow visualization: Toward a comprehensive flow diagnostic tool. *Int. Comp. Biol.* **42**, 964-970. doi:10.1093/icb/42.5.964
Godfrey, S. J. (1985). Additional observations of subaqueous locomotion in the California Sea Lion (*Zalophus californianus*). *Aqua. Mamm.* **11**, 53-57.
Gosline, J. M. and DeMont, M. E. (1985). Jet-propelled swimming in squids. *Sci. Amer.* **252**, 96-103. doi:10.1038/scientificamerican0185-96
Hanlon, R. T., Hixon, R. F. and Hulet, W. H. (1983). Survival, growth, and behavior of the loliginid squids *Loligo plei*, *Loligo pealei*, and *Lolliguncula brevis* (Mollusca: Cephalopoda) in closed sea water systems. *Biol. Bull.* **165**, 637-685. doi:10.2307/1541470
Hanlon, R. T. and Messenger, J. B. (2018). *Cephalopod Behaviour*. Cambridge: Cambridge University Press.
Hedrick, T. L. (2008). Software techniques for two-and three-dimensional kinematic measurements of biological and biomimetic systems. *Bio. Biomim.* **3**, 034001. doi:10.1088/1748-3182/3/3/034001
Hoar, J. A., Sim, E., Webber, D. M. and O'Dor, R. K. (1994). The role of fins in the competition between squid and fish. In *Mechanics and Physiology of Animal Swimming* (ed. L. Maddock, Q. Bone and J. M. V. Rayner), pp. 27-33. Cambridge: Cambridge University Press.
Hove, J. R., O'Bryan, L. M., Gordon, M. S., Webb, P. W. and Weihs, D. (2001). Boxfishes (Teleostei: Ostraciidae) as a model system for fishes swimming with many fins: kinematics. *J. Exp. Biol.* **204**, 1459-1471. doi:10.1242/jeb.204.8.1459
Howland, H. C. (1974). Optimal strategies for predator avoidance: the relative importance of speed and manoeuverability. *J. Theor. Biol.* **47**, 333-350. doi:10.1016/0022-5193(74)90202-1
Hui, C. A. (1985). Maneuverability of the Humboldt penguin (*Spheniscus humboldti*) during swimming. *Can. J. Zool.* **63**, 2165-2167. doi:10.1139/z85-318
Hurley, A. C. (1978). School structure of the squid *Loligo opalescens*. *Fish. Bull.* **76**, 433-442.
Ishikawa, M. (1929). On a new species of a luminous squid from the Sea of Japan. *Proc. Imper. Acad.* **5**, 51-54. doi:10.2183/pjab1912.5.51
Jastrebsky, R. A., Bartol, I. K. and Krueger, P. S. (2016). Turning performance in squid and cuttlefish: unique dual-mode, muscular hydrostatic systems. *J. Exp. Biol.* **219**, 1317-1326. doi:10.1242/jeb.126839
Jastrebsky, R. A., Bartol, I. K. and Krueger, P. S. (2017). Turning performance of brief squid *Lolliguncula brevis* during attacks on shrimp and fish. *J. Exp. Biol.* **220**, 908-919. doi:10.1242/jeb.144261
Kajitani, L. and Dabiri, D. (2005). A full three-dimensional characterization of defocusing digital particle image velocimetry. *Meas. Sci. Tech.* **16**, 790. doi:10.1088/0957-0233/16/3/022
Katija, K., Colin, S. P., Costello, J. H. and Jiang, H. (2015). Ontogenetic propulsive transitions by *Sarsia tubulosa* medusae. *J. Exp. Biol.* **218**, 2333-2343.
Kier, W. M. (1982). The functional morphology of the musculature of squid (Loliginidae) arms and tentacles. *J. Morph.* **172**, 179-192. doi:10.1002/jmor.1051720205
Kier, W. M. (1989). The fin musculature of cuttlefish and squid (Mollusca, Cephalopoda): morphology and mechanics. *J. Zool.* **217**, 23-38. doi:10.1111/j.1469-7998.1989.tb02472.x
Kier, W. M. and Smith, K. K. (1985). Tongues, tentacles and trunks: the biomechanics of movement in muscular-hydrostats. *Zool. J. Linn. Soc.* **83**, 307-324. doi:10.1111/j.1096-3642.1985.tb01178.x
Kier, W. M. and Thompson, J. T. (2003). Muscle arrangement, function and specialization in recent coleoids. *Berliner Paläobiologische Abhandlungen* **3**, 141-162.
Krueger, P. S. and Gharib, M. (2003). The significance of vortex ring formation to the impulse and thrust of a starting jet. *Phys. Fluids,* **15**, 1271-1281. doi:10.1063/1.1564600
Leahy, A. M., Fish, F. E., Kerr, S. J., Zeligs, J. A., Skrovan, S., Cardenas, K. L. and Leftwich, M. C. (2021). The role of California sea lion (*Zalophus californianus*) hindflippers as aquatic control surfaces for maneuverability. *J. Exp. Biol.* **224**, jeb243020. doi:10.1242/jeb.243020
Mather, J. A. and O'Dor, R. K. (1984). Spatial organization of schools of the squid *Illex illecebrosus*. *Mar. Freshw. Beh. Phy.* **10**, 259-271.
Moody, R. C., Helland, J. M. and Stein, R. A. (1983). Escape tactics used by bluegills and fathead minnows to avoid predation by tiger muskellunge. *Environ. Biol. Fish.* **8**, 61-65. doi:10.1007/BF00004947
Nesis, K. N. (1987). *Cephalopods of the World: Squids, Cuttlefishes, Octopuses, and Allies*. Neptune City, NJ: TFH Publications.
Nichols, A. R. (1905). On some Irish specimens of a large squid, *Sthenoteuthis pteropus* (Steenstrup). *Irish Naturalist,* **14**, 54-57.
O'Dor, R. K. (1988). The forces acting on swimming squid. *J. Exp. Biol.* **137**, 421-442. doi:10.1242/jeb.137.1.421
Packard, A. (1969). Jet propulsion and the giant fibre response of *Loligo*. *Nature,* **221**, 875-877. doi:10.1038/221875a0
Parson, J. M., Fish, F. E. and Nicastro, A. J. (2011). Turning performance of batoids: limitations of a rigid body. *J. Exp. Mar. Biol. Ecol.* **402**, 12-18. doi:10.1016/j.jembe.2011.03.010
Pereira, F. and Gharib, M. (2002). Defocusing digital particle image velocimetry and the three-dimensional characterization of two-phase flows. *Meas. Sci. Tech.* **13**, 683. doi:10.1088/0957-0233/13/5/305
Pereira, F. and Gharib, M. (2004). A method for three-dimensional particle sizing in two-phase flows. *Meas. Sci. Tech.* **15**, 2029. doi:10.1088/0957-0233/15/10/012
Pereira, F., Stüer, H., Graff, E. C. and Gharib, M. (2006). Two-frame 3D particle tracking. *Meas. Sci. Tech.* **17**, 1680. doi:10.1088/0957-0233/17/7/006
Roper, C. F. (1964). *Enoploteuthis anapsis*, a new species of enoploteuthid squid (Cephalopoda: Oegopsida) from the Atlantic Ocean. *Bull. Mar. Sci. Gulf Caribb.* **14**, 140-148.
Roper, C. F. (1968). Preliminary descriptions of two new species of the bathypelagic squid Bathyteuthis (Cephalopoda: Oegopsida). *Proc. Biol. Soc. Wash.* **81**, 161-172.
Saffman, P. G. (1992). *Vortex Dynamics*. Cambridge: Cambridge University Press.
Stewart, W. J., Bartol, I. K. and Krueger, P. S. (2010). Hydrodynamic fin function of brief squid, *Lolliguncula brevis*. *J. Exp. Biol.* **213**, 2009-2024. doi:10.1242/jeb.039057
Sugimoto, C., Yanagisawa, R., Nakajima, R. and Ikeda, Y. (2013). Observations of schooling behaviour in the oval squid *Sepioteuthis lessoniana* in coastal waters of Okinawa Island. *Mar. Biodiv. Rec.* **6**, e34. doi:10.1017/S1755267213000067

Sutherland, K. R. and Madin, L. P. (2010). Comparative jet wake structure and swimming performance of salps. *J. Exp. Biol.,* **213**, 2967-2975. doi:10.1242/jeb.041962

Sutherland, K. R., Gemmell, B. J., Colin, S. P. and Costello, J. H. (2019). Maneuvering performance in the colonial siphonophore, *Nanomia bijuga*. *Biomimetics,* **4**, 62. doi:10.3390/biomimetics4030062

Tang, M., Boisclair, D., Ménard, C. and Downing, J. A. (2000). Influence of body weight, swimming characteristics, and water temperature on the cost of swimming in brook trout (*Salvelinus fontinalis*). *Can. J. Zool.* **57**, 1482-1488.

Thandiackal, R. and Lauder, G. V. (2020). How zebrafish turn: analysis of pressure force dynamics and mechanical work. *J. Exp. Biol.,* **223**, jeb223230. doi:10.1242/jeb.223230

Vecchione, M. and Roper, C. F. (1991). Cephalopods observed from submersibles in the western North Atlantic. *Bull. Mar. Sci.* **49**, 433-445.

Walker, J. A. (1998). Estimating velocities and accelerations of animal locomotion: a simulation experiment comparing numerical differentiation algorithms. *J. Exp. Biol.* **201**, 981-995. doi:10.1242/jeb.201.7.981

Webb, P. W. (1991). Composition and mechanics of routine swimming of rainbow trout *Oncorhynchus mykiss*. *Can. J. Fish. Aquat. Sci.* **48**, 583-590. doi:10.1139/f91-074

Webb, P. W. (1997). Designs for stability and maneuverability in aquatic vertebrates: What can we learn? In *Tenth International Symposium on Unmanned Untethered Submersible Technology: Proceedings of the Special Session on Bio-Engineering Research Related to Autonomous Underwater Vehicles*, pp. 86-108. Durham, NH: Autonomous Undersea System Institute.

Webb, P. W. (2006). Stability and maneuverability. In *Fish Biomechanics* (ed. R. E. Shadwick and G. V. Lauder), pp. 281-332. San Diego: Academic Press.

Weihs, D. (1993). Stability of aquatic animal locomotion. *Cont. Math,* **141**, 443-461. doi:10.1090/conm/141/19

Weihs, D. and Webb, P. W. (1984). Optimal avoidance and evasion tactics in predator-prey interactions. *J. Theor. Biol.* **106**, 189-206. doi:10.1016/0022-5193(84)90019-5

Wu, J. Z., Ma, H. Y. and Zhou, M. D. (2007). *Vorticity and Vortex Dynamics*. Springer Science & Business Media.

York, C. A. and Bartol, I. K. (2016). Anti-predator behavior of squid throughout ontogeny. *J. Exp. Mar. Biol. Ecol.* **480**, 26-35. doi:10.1016/j.jembe.2016.03.011

Young, J. Z. (1938). The functioning of the giant nerve fibres of the squid. *J. Exp. Biol.* **15**, 170-185. doi:10.1242/jeb.15.2.170

Zuev, G. V. (1966). Characteristic features of the structure of cephalopod molluscs associated with controlled movements. *Fish. Res. Bd. Can.* **1011**, 1968.